https://doi.org/10.5194/essd-2026-653
Preprint. Discussion started: 25 September 2026

Open Access Earth System Science Data Discussions

MOISE station : Monthly environmental monitoring in the Southwestern lagoon of New Caledonia

Salomé Domergue[2], Martine Rodier[1], Cécile Dupouy[1], Maxime Duphil[2], David Varillon[3], Amandine Delepierre[3], Anne Desnues[4], Sylvie Fiat[2], Christophe Menkes[2,5]

[1]Aix Marseille, University of Toulon, CNRS, Institute of Research for Development (IRD), MIO, Marseille, France
[2]UMR 250 ENTROPIE, IRD, University of La Réunion, Ifremer, University of New Caledonia, Noumea, New Caledonia
[3]UAR 191 IMAGO, IRD, Noumea, New Caledonia
[4]UAR 191 LAMA, Centre IRD Bel-Air, Dakar, Sénégal
[5]EMR 9001 SantEco, CNRS, IRD, University of New Caledonia, Unversity of La Réunion, Promenade Roger-Laroque, 98848 Noumea Cedex, New Caledonia, France

Correspondence to: Salomé Domergue (salome.domergue@ird.fr)

Abstract. From July 2012 to December 2024, in the Southwestern lagoon of New Caledonia, the MOISE station (https://www.mio.osupytheas.fr/fr/moise-mouillage-lagonaire-instrumente-suivi-biogeochimique/, last access 26/08/2025) was surveyed with moored instruments and monthly visits providing unique long time series of hydrological and biogeochemical measurements in approximately 10m depth. The MOISE program objective was to characterize lagoon environmental variability across monthly, seasonal, and interannual timescales at a site potentially impacted by river outputs. Here we provided a 13-year quality-controlled dataset with vertical profiles of temperature, salinity, and chlorophyll-adjusted fluorescence from Conductivity-Temperature-Depth (CTD) and continuous currents from a moored 600 kHz Acoustic Doppler Current Profile (ADCP).

This site represents the unique location in New Caledonia lagoon to deliver an extended multi-parameter time series of long-term monitoring of the lagoon's environmental state and circulation dynamics. The length of the time series allowed the depiction of the ENSO impact (El Niño-Southern Oscillation) on the interannual variability. A clear seasonal cycle was also observed, with higher chlorophyll during austral summer when temperatures are highest, salinity lowest and wind-driven currents strongest and predominantly directed toward the west-northwest. MOISE data further highlight the strong influence of extreme events such as tropical cyclones, tropical depressions and heavy rainfall, on the lagoon, which can induce temporary stratification of the water column that is otherwise generally homogeneous.

The dataset was post processed, quality controlled and is available in netcdf on SEANOE in open access (SEA ScieNtific Open data Edition) at the following DOI : https://doi.org/10.17882/98821 (Rodier et al., 2026).

1 Introduction

Due to man-induced climate change, significant ocean changes have been observed worldwide over the past decades (Bindoff et al., 2019; Fox-Kemper et al., 2021). While large-scale global signal are captured by the observing systems as

https://doi.org/10.5194/essd-2026-653
Preprint. Discussion started: 25 September 2026

well as climate models, estimating regional changes remain challenging (Doblas-Reyes et al., 2021). In the Southwest Pacific, numerous islands of the PICTS (Pacific Island Countries and Territories) are particularly exposed to its impacts (Johnson and Wabnitz, 2025) and many countries are seeking to construct national adaptation plans to cope with these changes. However, in many PICTS EEZs, information on actual ocean trends and variabilities in coastal waters and lagoons remain limited. Existing monitoring initiatives provides key information on short-to-long-term coastal changes in temperature in a number of PICTS's lagoons, monitoring of additional parameters such as currents, chemical and biological parameters are often missing. Multi-parameter observations are essential to better apprehend climate change impacts on water quality and coastal ecosystems. Such observations can be conducted over a range of temporal scales, from short-term to long-term deployments.

Short term deployments on coral reef ecosystems which combined physical and biogeochemical measurements allowed to study lagoon variability (Grenz et al., 2010, and references therein) and associated processes such as primary production assessment (Rodier et al., 2024; Torréton et al., 2010), internal waves modulating thermal environment (Leichter et al., 2012; Reid et al., 2019; Wyatt et al., 2020), and circulation induced by ocean-lagoon exchanges (Bruyère et al., 2023, 2024). At longer timescales, observatories, defined here as monitoring systems providing measurements at fixed sites or across network, help to identify seasonal, interannual and climatic trends. From South Pacific to Indian ocean, ReefTEMPS coastal network (https://www.reeftemps.science/, last access : 07/08/2026), based on moored lagoon sensors, providing long-term physical observations whose oldest records date back to 1958 (Le Gendre et al., 2025). Moreover, some networks coupled physic and biology, such as the Moorea Coral Reef Long-term Ecological Research (https://mcr.lternet.edu/, last access : 07/08/2026) (Alber et al., 2013; Leichter et al., 2013) and CORAIL (https://observatoire.criobe.pf/CRIOBEData/) network in French Polynesia, which study long-term functioning of coral reef across lagoon and forereef habitats (Chancerelle et al., 2025). In this context, MOISE complements existing monitoring networks by providing long-term, high-frequency multiparameter observations of the lagoon of New Caledonia (NC).

In France, the SOMLIT network (https://www.somlit.fr/, last access 26/08/2025) focuses on monitoring and understanding the pluri-decadal evolution of coastal ecosystems, to determine how marine ecosystems respond to the combined effect of natural environmental and anthropic pressures (Cocquempot et al., 2019). Based on SOMLIT approach and its sampling strategy (https://www.somlit.fr/parametres-et-protocoles, last access 26/08/2025), MOISE (MOuillage Instrumenté et Suivi biogEochimique) program has been initiated, implemented in the Southwest lagoon of NC. With a regular survey, it provides a baseline to study the environmental variability and lagoon ecosystems dynamics under climate change.

MOISE station characterize the oligotrophic NC lagoon physical and biogeochemical natural and human-induced variability, by observing multiple parameters over more than 10 years (from July 2012 to December 2024) monitoring the whole water column (0 - 9.4 m) ranging from short term events to interannual scales. The full MOISE dataset includes continuous currents measurements, and monthly sampling of CTD profiles measuring temperature, salinity, fluorescence, turbidity, pH

https://doi.org/10.5194/essd-2026-653
Preprint. Discussion started: 25 September 2026

and photosynthetically active radiation (PAR) combined with surface (from 1 to 2 m) and bottom (from 6 to 7 m) water samples (e.g., nitrate, nitrite, phosphate, silicate), suspended organic matter, particulate organic carbon and nitrogen, stable isotopes of carbon and nitrogen, chlorophyll-a and phaeopigments, HPLC pigment composition, and phytoplankton and bacterial abundance (Dupouy and Rodier, 2026). Here we limited the study and assessment of the MOISE data to fully calibrated, quality-controlled measurements of currents measurements, temperature, salinity, fluorescence profiles and chlorophyll-a concentrations. While not presented in the study, additional raw data collected from Niskin bottle samples that are yet to be quality-controlled are available in the SEANOE repository https://doi.org/10.17882/98821 (Rodier et al., 2026).

The MOISE station was established with initial funding from GOPS (Grand Observatoire de l'environnement et de la biodiversité terrestre et marine du Pacifique Sud) in 2011. Since 2014, MOISE was supported by the Mediterranean Institute of Oceanography (MIO) of Marseille and the Observatoire des Sciences de l'Univers Pythéas (OSU Pytheas) with the help of the Research Support Unit IMAGO (Instrumentation, Analytical Facilities, Observatories in Geophysics and Oceanography) and the support of the French National Research Institute for Sustainable Development (IRD) of New Caledonia. Between August 2013 and June 2019, MOISE station complemented the ReefTEMPS network, which installed a reference station (e.g., BAKAUI01) at the MOISE site to continuously monitor temperature and salinity. MOISE monitoring ended in 2024 following the departure of the principal investigators from NC.

The paper is organized as follows: Section 2 describes the study area, including both general environmental forcings and those specific to the MOISE station. Section 3 presents the data collection methods, the procedures for data processing and formatting, and the quality control applied to the dataset for each instrument. Finally, section 4 provides an overview of some data observations.

2 The MOISE station: a coastal observation site in the Southwest lagoon of New Caledonia

2.1 Description of the study area

Located approximately 21°S in the Southwest Pacific, NC is surrounded by one of the largest barrier reef and and featured a wide diversity of lagoon geomorphology in the world. The MOISE station is located in the Southwest lagoon which is classified by the UNESCO as a world humanity heritage. This area is a wide semi-open coral reef lagoon (Ouillon et al 2010) extending from coastal bays and fringing reefs to the barrier reef and channels (Andréfouët et al., 2009). The station is located close to the Prony reef, a reef with depths ranging from 0 to 2 m, and approximately 13 km from the Dumbéa channel, which connects the lagoon to deeper oceanic waters.

https://doi.org/10.5194/essd-2026-653
Preprint. Discussion started: 25 September 2026

The MOISE station is located West of Nouméa, offshore from the Dumbéa Bay, near the transition between the Dumbéa River mouth (approximately 14.5 km offshore) and the Southwest lagoon. The site was selected to capture strong environmental events driven by freshwater and nutrient inputs from the Dumbéa River, particularly during extreme weather events possibly leading to plume development and specific algal blooms. This station is positioned at 22.2466°S, 166.3169°E (Fig. 1) and is installed on the Basse Kaui reef at a total water depth of 9.4 m (depth from the bottom to the surface). Surrounding lagoon depths generally range between 20 and 26 m, highlighting the contrast between the shallow reef-associated station site and the deeper lagoon areas nearby. Variability in the physico-chemical properties of the lagoon waters is strong, particularly during periods of high runoff (Fichez et al., 2010). This variability is also amplified by intense hydrodynamic processes, including tidal currents and wind-driven circulation (Douillet, 1998; Dumas et al., 2012; Duphil et al., 2025; Lefèvre et al., 2010; Ouillon et al., 2010), combined with terrigenous inputs resulting in high turbidity (Dupouy et al., 2023; Martias, 2018). The MOISE area, due to its position far from an estuary/coast, is weakly impacted by anthropogenic pressures, including the Noumea nickel processing plant located quite a distance away and rain-induced urban discharges (Dumbea disctrict).

https://doi.org/10.5194/essd-2026-653
Preprint. Discussion started: 25 September 2026

Open Access Earth System Science Data Discussions

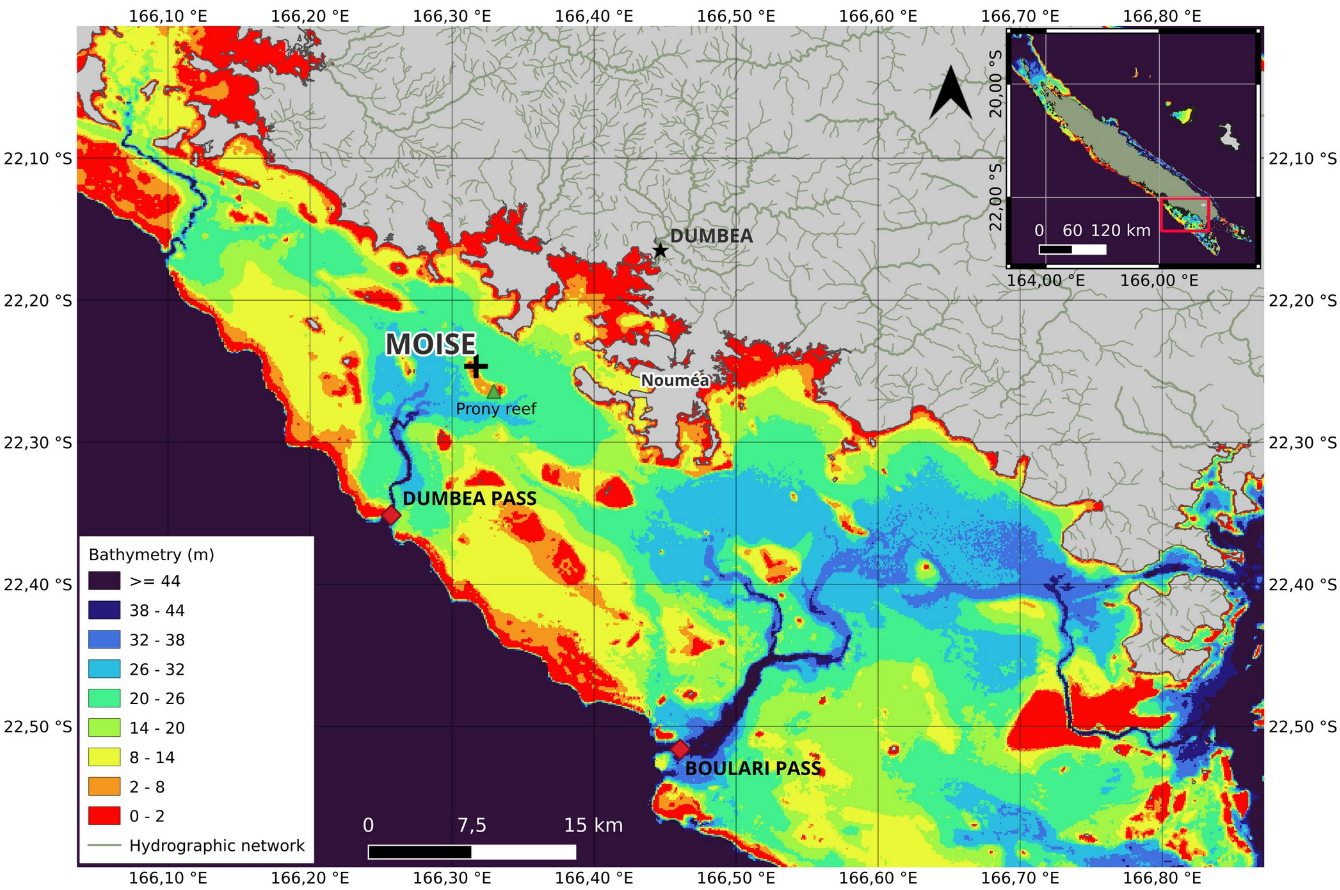

Figure 1: Geographical setting of the MOISE Station, in the Southwestern lagoon of New Caledonia, under the influence of the Dumbéa river. The bathymetry is represented as color contours. Hydrographic network is used to represent the river, land and coastlines . Bathymetric data obtained from the TSUCAL project (https://dx.doi.org/10.17183/MNT_NC100m_TSUCAL_WGS84, last access : 26/08/2025). Hydrological data are provided by the Government of New Caledonia / DAVAR / SDE / MERE (Mesures et Etudes de la Ressource en Eau) (https://data.gouv.nc/explore/dataset/hydrometrie/information/), last access : 26/08/2025) from GEOREP site (https://georep.nc/plate-forme-de-telechargement, last access : 26/08/2025).

2.2 Climatic and oceanic forcing conditions from New Caledonia to MOISE station

New Caledonia is characterized by a tropical climate with marked seasonal variability, largely influenced by the seasonal migration of the South Pacific Convergence Zone (SPCZ), a major convective zone extending diagonally across the Southwest Pacific (Vincent et al., 2011). During the austral summer (December–March), the SPCZ shifts southward, bringing warm temperatures and enhanced rainfall to NC. In austral winter (June–September), the SPCZ retreats northward, resulting in cooler and drier conditions over the archipelago (Ceccarelli et al., 2013; Payri et al., 2019).

https://doi.org/10.5194/essd-2026-653
Preprint. Discussion started: 25 September 2026

The dominant wind regime in NC is the Southeast trade wind system (~ 70-80 % of wind regimes), which prevails from October to May with average speeds of around 8 m s⁻¹ (Pesin et al., 1995, Lefèvre et al., 2010), and weakens during austral winter (Ouillon et al., 2005). Four distinct wind regimes have been identified during austral summer (November to April) (Lefèvre et al., 2010) : 1) strong and steady south-east trade winds, quasi-permanent throughout the season; 2) short-lived weak and highly variable easterly trade winds bringing warm and humid air and frequent rainfall ; 3) south-westerly winds and typically occurs at the end of the austral summer and 4) dry south-east trade winds, generally weak but stronger in the north, occurring mainly at the end of the austral winter and early summer and bringing drier conditions over NC. Although Southeasterly trade winds dominate the regional circulation, other wind regimes can occur. Westerly winds are occasionally observed during the cool season and are associated with the passage of cold fronts, linked to cyclonic low-pressure located 500km south (Dutheil et al., 2021; Specq et al., 2020). Although less frequent than south-easterly trade winds, they are often associated with strong rainfall affecting the Western and Southern part of NC (Pesin et al., 1995).

Superimposed on this seasonal cycle, the regional climate is also modulated by large-scale climate variability, such as the Madden–Julian Oscillation at intraseasonal timescales and the El Niño–Southern Oscillation (ENSO) at interannual scales. ENSO occurs every 2 - 8 years (around every 4 years on average). In summer, El Niño brings drier (10-40 % less rainfall), and cooler conditions (~ -0.5 – 1 °C), whereas, La Niña brings warmer (~ +0.5 - 2 °C) and wetter conditions (around 10 - 30 % more rainfall) (Menkès, 2012). ENSO is a main driver of interannual variability in temperature and especially rainfall in the region (Barbero and Moron, 2011; Dutheil et al., 2021; Moron et al., 2016). That large-scale climate fluctuation also influences the regional atmospheric circulation.

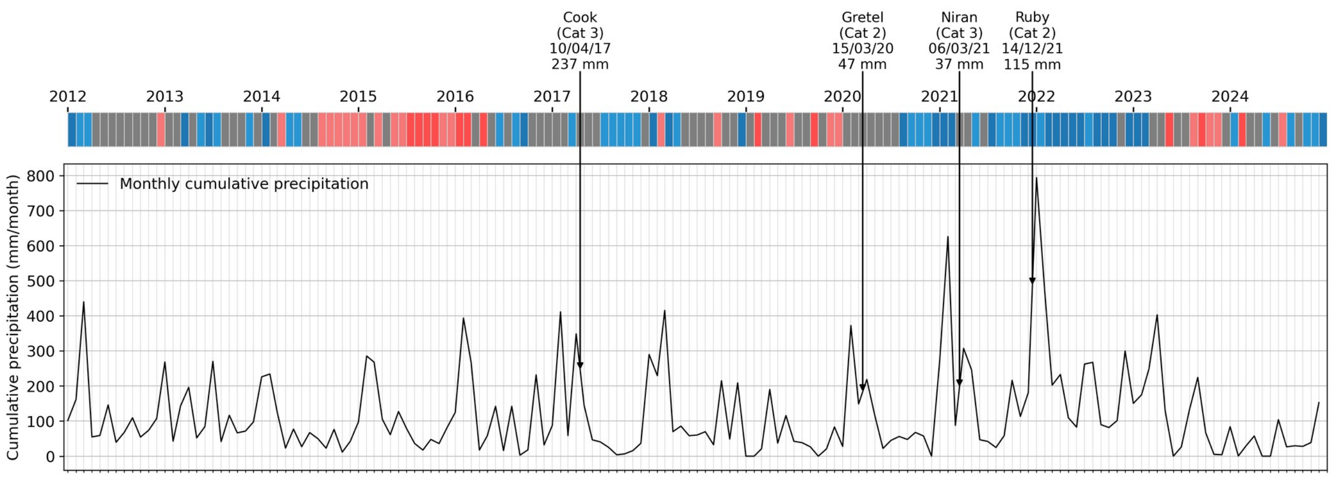

Figure 2: Timeline of extreme events influencing the parameters measured at the MOISE station, including ENSO phases (represented by colored bars: blue for El Niño and red for La Niña, with color intensity indicating event strength (strong El Niño

https://doi.org/10.5194/essd-2026-653
Preprint. Discussion started: 25 September 2026

(index ≤ −1), El Niño (−1 < index ≤ −0.5), neutral (−0.5 < index < 0.5), La Niña (0.5 ≤ index < 1), and strong La Niña (index ≥ 1)), cyclones and tropical depressions with the associated precipitation accumulation. The lower panel shows the monthly cumulative precipitation time series (mm/month) derived from hourly records at the Dumbéa station. Data sources : NOAA (http://www.cpc.ncep.noaa.gov/data/indices/soi, last access 26/08/2026), Météo NC, Météo-France.

Fig. 2 illustrates the range of climatic and meteorological conditions affecting the MOISE station during the observation period. Here we focused on different timescales of atmospheric variability ranging from short-lived events to interannual variability. The interannual variability due to ENSO phases was determined from NOAA's monthly Southern Oscillation Index (SOI) dataset (https://www.ncei.noaa.gov/access/monitoring/enso/soi, last access: 26/08/2025). Between July 2012 and December 2024, El Niño episodes occurred from mid-2015 to mid-2016 and again from mid-2023 to mid-2024. The most significant La Niña events extended from mid-2017 to mid-2018, from mid-2020 to early 2023 (often depicted as the exceptional multiyear La Niña (Wang et al., 2023) and from mid-2024 to the end of 2024. Monthly cumulative precipitation highlighted periods of intense rainfall events, particularly at the beginning of 2021 and between late 2021 and early 2022 during the exceptional La Niña . Over the January-February period in 2022, the Dumbéa station recorded 1657 mm of rainfall, about seven times the 1991-2020 climatological cumulative rainfall of 235.5 mm (107.2 mm in January and 128.3 mm in February) at Nouméa (Météo-France, https://donneespubliques.meteofrance.fr/FichesClim/FICHECLIM_98818001.pdf). This period corresponded to one of the most intense rainfall episodes observed during the study period.

New Caledonia is characterized by a predominantly semidiurnal tidal regime, driven by the M_2 constituent, the main harmonic with a period of approximately 12.4 h. Tidal currents within the lagoons are generally weak, with typical velocities of about 0.05-0.10 m s^{-1}, although locally stronger currents occur near reef channels (Douillet, 1998; Bruyère et al., 2022). The complex NC reef geomorphology modifies the propagation of tidal waves, resulting in spatial variations in both tidal phase and amplitude (Douillet, 1998; Ouillon et al., 2010). Consequently, phase shifts of several tens of minutes and amplitude differences of several centimeters may develop within narrow lagoon sectors (Duphil et al., 2025) and semi-enclosed coastal bays.

In addition to tidal forcing, water circulation in the southwestern lagoon is influenced by oceanic inflows through reef channels and by freshwater inputs from adjacent watersheds (Douillet et al., 2001; Ouillon et al., 2010). Within our study area, the Dumbéa River represents the main source of freshwater, as indicated by the hydrographic network provided by the Gouvernement de la Nouvelle-Calédonie / DAVAR / SDE / MERE (Mesures et Études de la Ressource en Eau) dataset (Fig. 1). River discharge and surface runoff are sustained by relatively high rainfall, with annual precipitation exceeding 2,100 mm in parts of the region (Terry and Wotling, 2011).

Along the west coast, the energetic seasonal swell predominantly approaches from the Southwest and is characterized by significant wave heights exceeding 2.0 m and peak periods longer than 12 s (Pagli et al., 2024). These swells are primarily

https://doi.org/10.5194/essd-2026-653
Preprint. Discussion started: 25 September 2026

generated in the Tasman Sea and become more frequent during the austral winter. New Caledonia is also periodically affected by extreme meteorological events, particularly tropical cyclones, which occur mainly during the cyclonic season from November to April (Bonvallot et al., 2012; Payri et al., 2019). Tropical cyclones account for less than 30% of extreme-wave events along the southwestern lagoon, indicating that intense non-cyclonic swell events also play a major role in the regional wave climate (Pagli et al., 2024). As offshore waves approach the lagoon, they undergo substantial transformation and dissipation through breaking over the barrier reef. This process generates wave setup and wave-driven currents across the reef crest and in the back-reef environment (Duphil et al., 2025). During energetic meteorological events, enhanced wave-driven resuspension of bottom sediments and increased river discharge can substantially increase turbidity, while freshwater inputs reduce coastal salinity (Rougerie, 1986; Bruyère et al., 2022).

During the MOISE observation period, several extreme meteorological events affected the study area. The most extreme short-term variability occurred mainly during cyclones and tropical depressions. These were labeled based on Météo-France records (https://www.meteo.nc/nouvelle-caledonie/cyclone/climatologie-des-cyclones, last access: 26/08/2025). To illustrate the MOISE dataset on these scales, we selected two tropical cyclones (e.g., Cook and Niran, cat. 3) and two tropical depressions (e.g., Gretel and Ruby, cat. 2) on Fig. 2. For each event, we extracted the daily rainfall recorded at the Dumbéa meteorological station (166.481167°E-22.135833°S), defined as the cumulative precipitation measured on the day of the closest passage to the station from Météo-France dataset (https://www.data.gouv.fr/organizations/meteo-france/datasets): Cook (10 April 2017, 237 mm), Niran (6 March 2021, 37 mm), Gretel (15 March 2020, 47 mm), and Ruby (14 December 2021, 115 mm).

3 MOISE in-situ oceanographic observations

In this section, we describe the MOISE dataset acquired over 13 years (from January 2012 to December 2024), the collecting methods and the calibrations procedures. An overview of the instrumentation timeline is illustrated in Fig. 3.

https://doi.org/10.5194/essd-2026-653
Preprint. Discussion started: 25 September 2026

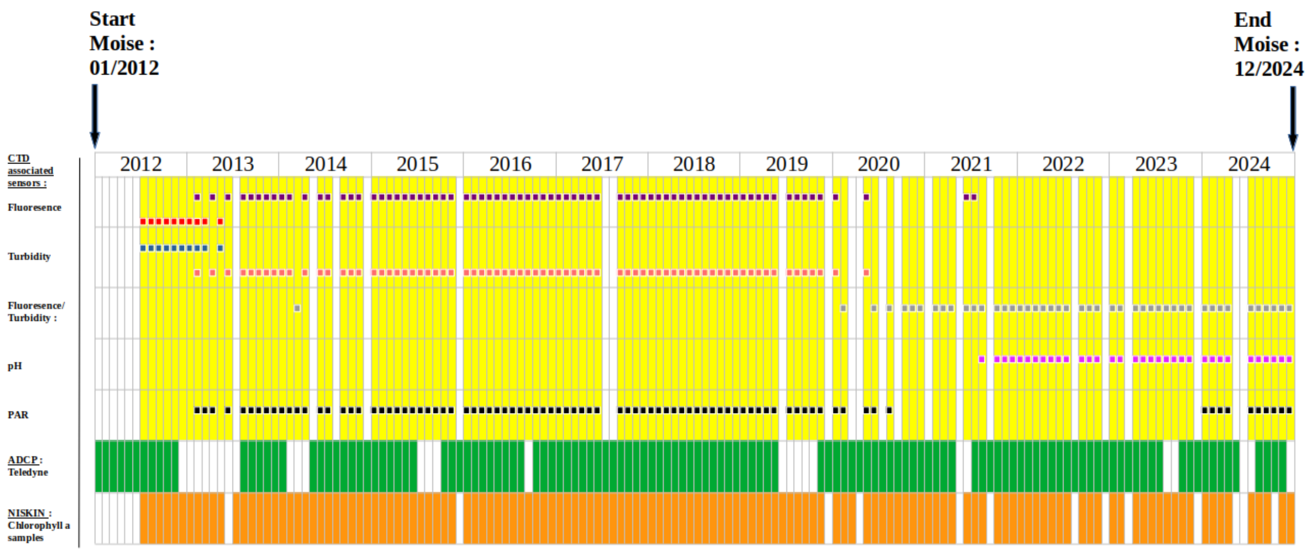

Figure 3: Timeline of instrumentation and sampling at the MOISE station during the MOISE observational period. CTD profiles (SBE 19plus, SEABIRD) are shown in yellow with their associated sensors : fluorescence sensors : WET Labs/ WETstar (purple) and WET Labs ECO-AFL/FL (red), Turbidity sensors : Upoly 0 (zero-order polynomial calibration) (blue) and Seapoint (pink), Fluorescence/turbidity : WET Labs ECO (grey), pH : SBE 18, Seabird (magenta) and PAR (photosynthetically active radiation) : Irradiance, Biospherical/Licor (black). Current measurements from the 600 kHz ADCP (Workhorse Sentinel, Teledyne) are shown in green. Chlorophyll a sample from Niskin bottles are shown in orange.

All collected data were finally produced in NetCDF or CSV format using Python, formatted following OceanSITES conventions (https://repository.oceanbestpractices.org/handle/11329/387, last access : 26/08/2025). Variables names followed the NERC vocabulary P09 (https://vocab.nerc.ac.uk/collection/P09/current/, last access : 26/08/2025). All ADCP and CTD datasets are finally provided at processing state 1B. The processing state codes, described in Table E1 (Appendix E), indicate the level of data processing applied, which includes sensor calibration, visual inspection of the data, and the application of quality control procedures resulting in Quality Control (QC) flags which are described in Table D1 (Appendix D) for the measured variables). In addition to CTD and ADCP profiles, two datasets from Niskin water sampling are provided. The first dataset is delivered at processing level 1B and contains only the quality-controlled chlorophyll-a measurements derived from water sampling.

3.1 ADCP currents measurements

3.1.1 Instrumentation and deployment and data acquisition

An 614.4 kHz, upward-facing Acoustic Doppler Current Profiler of the Workhorse Sentinel model (https://www.teledynemarine.com/en-us/products/SiteAssets/RD%20Instruments/wh_ii_datasheet_04_2023.pdf, last access : 11/06/2026), manufactured by Teledyne RD Instruments (serial no. 7691), was moored on a stable platform (Fig. 4) from

https://doi.org/10.5194/essd-2026-653
Preprint. Discussion started: 25 September 2026

Open Access Earth System Science Data Discussions

March 2011 to December 2024, with an average immersion depth of 8.3 m below the sea surface, estimated from the ADCP pressure sensor measurements. For consistency with the CTD and Niskin bottle datasets, this paper focuses only on data collected between January 2012 and December 2024. The instrument ("Janus" configuration) has four beams angled at 20° from the longitudinal instrument axis to measure current velocities throughout the water column (https://www.teledynemarine.com/en-us/support/SiteAssets/RDI/Manuals%20and%20Guides/General%20Interest/BBPRIME.pdf, last access : 11/06/2026).

The UAR IMAGO team, certified iso-9001 since 2006 was responsible for managing the instrumentation since June 2014 and handled maintenance and configuration tasks for each deployment.

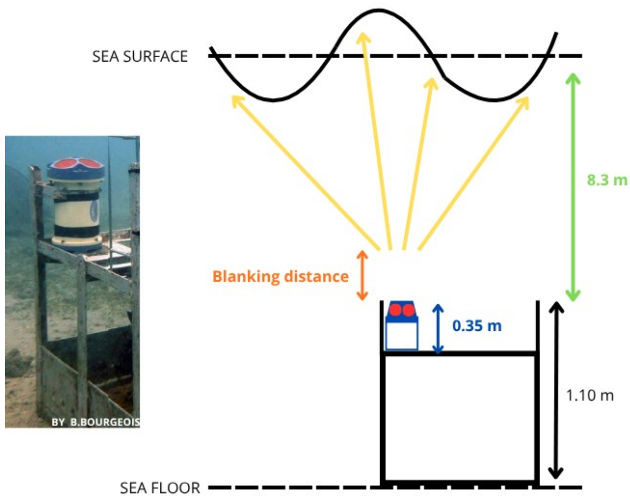

Figure 4: Deployment configuration of the upward-looking ADCP. The left panel shows the instrument mounted on a metal frame deployed on the seabed (photograph by B. Bourgeois). The right panel provides the schematic representation of the ADCP deployment, the yellow arrows represent the emitted acoustic beams. The instrument is installed approximately 8.3 m below the sea surface and the supporting stable platform is 1.10 m high. The blanking distance indicates the near-field region above the ADCP where velocity measurements cannot be obtained. Dashed lines represent the mean sea surface and the seabed and the black line indicates the water level. The schematic is not drawn to scale.

The ADCP is equipped with six auxiliary sensors: a heading sensor, two tilt sensors, a depth sensor, a temperature sensor and a pressure sensor. Measurements were performed in "burst" mode every 15 minutes with burst duration of 4 minutes and 50 seconds. The 4 beams of the ADCP measured acoustic echo intensity (backscatter) from which the ocean currents were derived (https://www.teledynemarine.com/en-us/support/SiteAssets/RDI/Manuals%20and%20Guides/General%20Interest/BBPRIME.pdf, last access : 11/06/2026). The instrument horizontal error for velocity measurement was 0.3% of water velocity relative to ADCP ± 0.3 cm s^{-1} as stated by the constructor.

Different ADCP configuration settings were applied over the MOISE period. This configuration parameters are described in Table 1; the blanking distance corresponds to the distance from the acoustic plates beyond which the data can be used and the number of bins determines the total distance sampling of the water column.

https://doi.org/10.5194/essd-2026-653
Preprint. Discussion started: 25 September 2026

The velocity data are provided at the native vertical resolution of the instrument. Depths in the dataset are expressed as distances from the ADCP transducer and therefore correspond to the measurement range above the instrument.

Period (UTC)	Blanking distance (m)	Ping interval (min:s)	Number of cells	Pings per ensemble	First bin distance (m)	Cell size (m)
Aug 2013 – May 2014	0.88	04:50	29	200	1.62	0.5
May 2014 – Aug 2014	0.50	03:60	19	250	1.22	0.5
Sep 2014 – Oct 2019	0.88	04:50	29	200	1.62	0.5
Nov 2019 – Oct 2022	0.88	04:50	25	200	1.62	0.5
Nov 2022 – Dec 2024	0.50	04:50	25	200	1.24	0.5

Table 1: ADCP Configuration settings used during the MOISE Observation Period

As recommended in the RDI manual, the ADCP setup involved two main calibrations steps: compass demagnetization and calibration to ensure accurate heading measurements.

Due to the battery life limitations and biofouling contamination, the ADCP was retrieved every three months for cleaning and data retrieval. It was redeployed less than 5 days later ensuring continuity in the current measurements. After each recovery, maintenance and configuration procedures were performed following the guidelines described in the WorkHorse Sentinel, Monitor, & Mariner Operation Manual (https://www.teledynemarine.com/en-us/support/SiteAssets/RDI/Manuals%20and%20Guides/Workhorse/WorkHorse_Operation_Manual.pdf; last access : 26/08/2025), including verification of the transducers, compass, and internal components.

During the instrument configuration, several treatments were applied. Zero pressure configuration was applied to pressure data, in order to subtract the standard atmospheric pressure (1013 hPa) and obtain relative pressure values referenced to the sea surface. Consequently, the pressure measurements reflected changes in sea level and were not affected by variations in atmospheric pressure.

In our configuration, the ADCP was set to earth coordinates, meaning that the velocity components were expressed as East, North, and Vertical components relative to the Earth's reference frame. The heading corrections were applied as well as pitch and roll corrections. This configuration allowed the velocity data to be directly interpreted in geographical coordinates, which is recommended for most oceanographic applications.

A magnetic declination correction of 12° was applied to convert the ADCP heading from magnetic north to true north. This correction was propagated to the horizontal velocity components, EWCT (Eastward Current) and NSCT (Northward Current).

3.1.2 Data processing and standardization

Raw data from the .000 binary raw data file were processed using a Python script based on the pycurrents_ADCP_processing library (https://github.com/IOS-OSD-DPG/pycurrents_ADCP_processing/tree/master/

Open Access Earth System Science Data Discussions

pycurrents_ADCP_processing; last access 26/08/25). This library, available on GitHub, created NetCDF outputs of the raw data files.

Dataset filenames read as follows: OS_BAKAUI_<YYYYMM>_<YYYYMM>_<XX>_<ZZ>_ADCP.nc where : OS : OceanSites naming convention, BAKAUI : name of the platform, YYYYMM_YYYYMM : date of the first and the last cycle measurement (year, month), XX : version file and ZZ : processing state as defined in Table D1 of Appendix D.

Variables included in the ADCP NetCDF files are described in Table F1 of Appendix F and are associated with quality control variables (“Variable”_QC) and complementary variables (listed in Table F3 of Appendix F).

3.1.3 Quality control

An initial quality control was applied to eastward and northward current data using the pycurrents_ADCP_processing library. This library used the water_depth value provided in metadata, set to 8.3 m, as the sea-surface threshold, with 0 m referenced to the acoustic transducers position. All values located above this threshold, corresponding to bins strictly above bin 17, were therefore flagged as bad data with a quality flag of 4 (see Fig. 4).

An additional quality-control procedure was applied to identify measurements affected by surface echoes. Upward-looking ADCPs do not provide reliable water velocity measurements near the surface due to acoustic surface side-lobe reflections, called side-lobe contamination. A common empirical rule, based on beam geometry, indicates that, for a 20° beam angle, data in the 6% or greater near-surface bins may be contaminated. In our processing, due to this side-lobe effect, the surface contamination distance was estimated from excessive current-direction changes between consecutive 0.5 m bins near the surface, inspired by (U.S. Integrated Ocean Observing System, 2019). When the directional difference exceeded 10°, the corresponding measurements were assigned a quality flag of 6 in EWCT_QC, NSCT_QC, and SAMA_QC.

After applying the quality control procedures to the current velocity data, we then processed the temperature and pressure variables. Following Blázquez-García et al., 2021, several outlier detection methods were applied as follows:

(1) Threshold-based anomaly detection ; Temperature values outside the range 15 °C to 35 °C were flagged as 4 “bad data”.

(2) Local outlier detection ; Spikes in the temperature time series were detected using a method similar to the Argo real-time quality control spike test, which compares each observation with the mean of its adjacent values (Wong et al., 2025). Data exceeding a threshold of 0.3 were flagged as anomalous.

(3) Robust sliding-window outlier detection; A Hampel filter (Toribio et al., 2025) was applied, based on the local median and the Median Absolute Deviation (MAD) to estimate the local dispersion. Observations deviating from the local median by more than four robust standard deviations were flagged as outliers.

(4) Residual-based anomaly detection using inter-sensor comparison; we used the difference between the ADCP temperature measurements and the ReefTEMPS SBE56 temperature record deployed at BAKAUI01 station (same position as MOISE

https://doi.org/10.5194/essd-2026-653
Preprint. Discussion started: 25 September 2026

station) (Le Gendre et al., 2025). Outliers were identified using a MAD criterion applied to the residuals of the difference between the time series. Observations exceeding three times the robust standard deviation ($\sigma = 1.4826 \times MAD$; Leys et al., 2013) were flagged at 4.

Fig. G1 and Fig. G2 in Appendix G show the MOISE and ReefTEMPS temperature time series, respectively, before and after quality control.

A quality control procedure was then applied to the pressure time series to identify potential instrument-related offsets. The pressure record was filtered to reduce tidal variability and highlight lower-frequency signals, then analysed using the Python library ruptures for change-point detection. Periods affected by detected offsets were assigned a quality flag of 4.

3.2 CTD measurements

3.2.1 Instrumentation, deployment and data acquisition

During the entire 12-year monitoring period, CTD profiles and bottle sampling were used to measure the vertical properties of the water column at MOISE. Monitoring was conducted monthly (Fig. 3), with two additional high-frequency monitoring periods involving daily measurements to capture short-term variability: from 16 to 27 July 2012 (austral winter) and from 17 to 28 February 2013 (austral summer) as part of the VAHINE project (Saulia et al., 2020). In the end, some gaps in data acquisition of CTD profiles and water sampling occurred due to equipment maintenance, field constraints or interruptions caused by the COVID-19 pandemic and the events of 2024 as summarized in table A1 in Appendix A.

CTD profiles were performed with Sea-Bird SBE19plus instruments (https://www.seabird.com.sbe-19plus-v2-seacat-profiler-ctd/product-downloads?id=60761421596, last access 26/09/2025). Two CTD profilers with their specific sensors serial numbers were mainly used: the UAR IMAGO's CTD, and MIO's CTD. On three occasions, IFREMER (French Research Institute for Exploitation of the Sea)'s CTD and AEL (Environmental testing and Assessment Laboratory)'s CTD were used as spare instruments while the usual CTD was under calibration. The CTDs operated in profiling mode with a sampling rate of 4 scans per second (4Hz) and measured temperature, conductivity, and pressure. Additional external sensors were mounted on the CTD frame depending on the deployment period (see Fig. 3 for the timeline of sensor usage) to measure fluorescence, turbidity, photosynthetically active radiation (PAR) and pH. Fluorescence was measured using a Wetlabs WETStar fluorometer (from SeaBird). Turbidity was measured using a Seapoint sensor and a sensor with zero-order polynomial calibration (Upoly 0). Around 2020, these two sensors were replaced by a unique WET Labs ECO-AFL/FL sensor, which combined fluorescence and turbidity measurements. PAR was measured using a Biospherical/Licor sensor and PH was measured using an SBE 18 pH sensor. The description of the associated sensors used on SBE19plus CTD probes is describe in Table B1 in Appendix B.

https://doi.org/10.5194/essd-2026-653
Preprint. Discussion started: 25 September 2026

The CTD instruments were returned to Seabird every three years for full factory calibration based on the Seabird SBE19plus manual (https://www.comm-tec.com/prods/mfgs/SBE/manuals_pdf/SBE19plusV2_002.pdf ; last access: 11/06/2026). The WET Labs ECO-AFL/FL sensor measuring fluorescence and turbidity mounted on the CTD since 2020 was returned for full factory calibration every five years. The pH sensor (last years) was calibrated monthly as described by the constructor note 18-2 in "SBE 18, 22, 27, and 30 pH Sensor Storage, Maintenance, and Calibration manual" (https://www.seabird.com/application-notes ; last access: 26/08/2025).

3.2.2 Data processing and standardization

For each CTD cast, conversion of .cnv to NetCDF files were performed by a Python script.
Dataset file names read as follows: OS_BAKAUI_<YYYYMMDD>_<XX>_<D/U>_<ZZ>_CTD.nc or .csv where : OS : OceanSites naming convention, BAKAUI : name of the station, YYYYMMDD : date of the profile ,XX : profile number, D/U : indicated the direction of the profile : D for downcast, U for upcast and ZZ : processing state.
Each NetCDF file contained the measured and calculated variables, referred to Table E2 of Appendix E.

Variables included in the CTD files are described in Table E2 of Appendix E and are associated with quality control variables ("Variable"_QC) and complementary variables (listed in Table E3 of Appendix E).

3.2.3 Quality control

A general data quality control was applied to identify and remove extreme outliers for each physical parameter dataset. Outliers were detected using the Interquartile Range (IQR; 25–75% of the distribution) method. The IQR was define as :

$$IQR = Q3 - Q1 \, , \tag{1}$$

Where Q1 and Q3 correspond to the 25th and 75th percentiles, respectively. Values lower or greater than X vas flagged as bad data "4". X defined as:

$$X = Q1 - 1{,}5 * IQR \, , \tag{2}$$

and

$$X = Q3 + 1{,}5 * IQR \, , \tag{3}$$

For salinity (PSAL) and conductivity (CNDC) data, the quality control procedure identified sensor malfunctions during several CTD casts, specifically on 23 May 2022 (casts 01 and 02), 26 June 2022 (cast 01), and 25 July 2022 (cast 01). For all these affected profiles, these data were flagged as bad data (quality flag = 4).

Additional quality control procedures were applied to the fluorescence data. Considering fluorescence as a proxy of chlorophyll-a, a threshold was defined based on previously reported chlorophyll-a values in the Southwest lagoon of New Caledonia. Fichez et al. (2010) reported maximum lagoon concentrations of approximately 0.8 mg m^{-3}, particularly near coastal areas. In our MOISE dataset, the highest chlorophyll-a value retained from the fluorescence sensor calibration curve was 0.91 mg m^{-3}. This range is also consistent with observations reported by Meyneng et al. (2024) after a cyclone event, where values near the MOISE area remained below 1 mg m^{-3}. Based on these observations and visual inspection of the dataset, a maximum threshold of 1.0 mg m^{-3} was applied.

A final quality control and calibration procedure was carried out using *in-situ* chlorophyll-a concentrations derived from water samples. These samples were collected at two depths between 1 and 2 m (surface) and between 6 and 7 m (near the bottom) using a Niskin bottle (see Fig. 3). Chlorophyll-a concentrations were determined following the methanol extraction and fluorometric analysis method described in Raimbault et al. (2004) and flagged as “probably good data” (flag = 2). For each monthly measurement, the mean fluorescence was calculated by averaging the CTD fluorescence data over the same depth ranges (1-2 m and 6-7 m) to align with the Niskin sample depths. Linear regressions were then established between the *in-situ* chlorophyll-a concentrations (averaged at the two depths) and the corresponding CTD fluorescence values. The regression coefficients, along with their R^2 and p-values, are presented in Table C1 (Appendix C).

In cases where the regression coefficients were not statistically robust (p-value > 0.05), an alternative calibration method was applied using a chlorophyll-a to fluorescence ratio. This ratio was subsequently applied to the fluorescence measurements to obtain adjusted values, with the ratio coefficients reported in Table C2 (Appendix C).

The overall linear fit between *in-situ* chlorophyll-a and fluorescence ($R^2 = 0.79$, p-value < 0.001) was significant, enabling the conversion of fluorescence into chlorophyll-a equivalents using the derived fit (see Figure 8 and Sect. 5.3 for the corresponding curves). In the dataset, this adjusted variable is labeled as "FLU2_ADJUSTED".

4 Overview of observations

In this section, we present the few key results from observations from the MOISE station dataset to highlight timescales from longer term variations to extreme event response.

For ADCP data, measurements flagged as 4 (“bad value”) or 6 (“additional qualification”) were masked. For CTD data, measurements flagged as 4 (“bad value”) and 3 (“probably bad value”) were also masked.

Chlorophyll-a data obtained from Niskin bottle samples were all retained.

4.1 Current patterns and wind regime influence

https://doi.org/10.5194/essd-2026-653
Preprint. Discussion started: 25 September 2026

Open Access Earth System Science Data Discussions

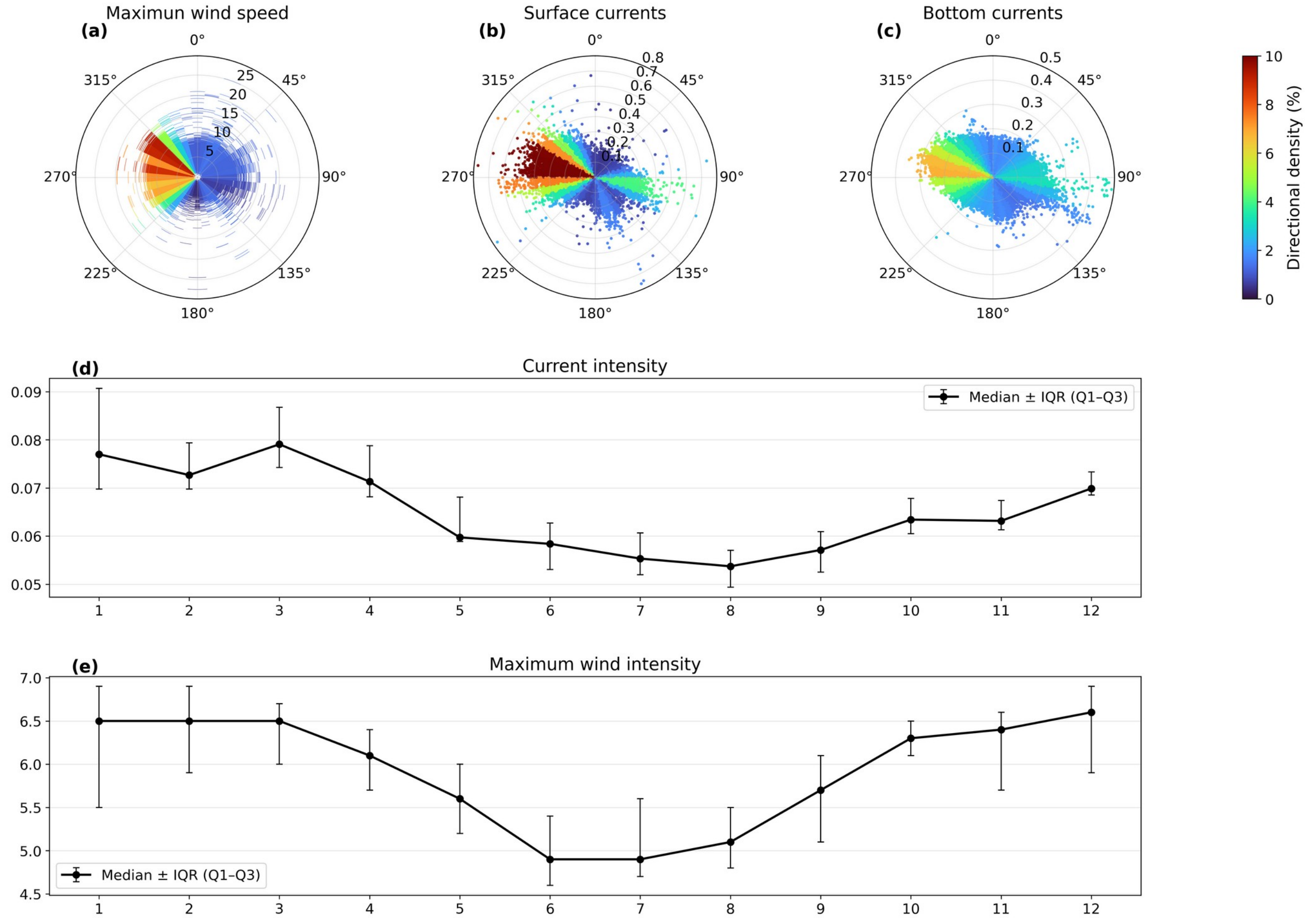

Figure 5: Directional distribution and intensity of daily maximum wind speed (10 min mean at 10 m) at the Faubourg Blanchot, Nouméa station (22°2761 °S, 166.4528 °E). Over the 01/2012-12/2024 period. (b) Directional distribution and intensity of currents at the surface (between 0,61 and 1,61 m ± 0,19 m below the surface) and (c) near the bottom (between 6,61 and 7,61 m ± 0,19 m below the surface). The angles in the roses indicate the direction to where the current and the wind flows (0° = North, 90° = East, 180° = South, 270° = West) and the circles represent the current intensity. Note that the direction convention chosen for the ocean currents and winds is identical. The values for each angle bin are expressed in % of the 0-360° circle to illustrate which direction dominates in proportion to other directions. (d) Monthly seasonal variability of current intensity (black curve) with vertical bars indicating the interquartile range (Q1–Q3) of the measurements entering the calculation of the monthly climatology.

The distribution of maximum wind speed direction binned in 10° sectors is shown in Fig. 5a. It reveals a dominant west-northwest direction, accounting for ~10 % of the observations compared to other sectors. The wind dominant direction is characteristic of the trade winds (Lefevre et al., 2010). Currents intensity and direction are represented by two roses of ADCP currents in Fig. 5b and 5c for the near-surface and near-bottom layers also binned into 10° sectors with the same direction convention as for the winds (Fig. 5a). Note that the convention for direction is chosen as for the currents (see legend and next paragraph), which is rotated by 180 ° compared to the usual meteorological convention.

https://doi.org/10.5194/essd-2026-653
Preprint. Discussion started: 25 September 2026

Both panels (in Fig. 5b and 5c) display a bimodal directional distribution. The upper-layer currents between 0.61 and 1.61 m ± 0,19 m below the sea-surface (called "near-surface currents"), showed stronger directional organization ~3 times higher velocities (mean of ~ 0,16 m s⁻¹, not shown) than the bottom layer (called "near-bottom currents"), at depths between 6,61 and 7,61 m ± 0,19 m (mean ~ 0.06 m s⁻¹, not shown). They were predominantly oriented toward the west-northwest direction, which accounted for more than 10 % of occurrences and a secondary main direction toward the east, representing about 5 % of occurrences. Currents speeds in the near-surface layer often reached up to 0,6 m s⁻¹, with occasional peaks above 0,8 m s⁻¹. Near-bottom currents were mostly below 0,2 m s⁻¹ in the west-northwest direction, and up to 0,4 m s⁻¹ in the eastward direction. The current roses reveal a marked vertical structure, with a dominant west-northwest direction broadly aligned with the wind and a weaker secondary eastward flow opposing the wind direction. The roses further show that near-surface currents are deflected by approximately 15 ° to the west relative to the wind direction, and near-bottom currents are deflected by ~ 10 ° westward to surface direction.

These observations suggest that the dynamics of the system are mainly controlled by wind forcing. The resulting current structure appears to be modulated by vertical shear arising from the combined effects of surface wind stress and bottom friction. The progressive change in direction from the wind to the near-surface and from the near-surface to the near-bottom currents, indicates a vertically sheared response that may be induced by the Coriolis force with a vertical rotation of the current in the water column in response to Ekman effect (Roach et al., 2015). This interpretation is consistent with Ouillon et al. (2010), who showed that the coupling of wind- and tide-driven hydrodynamics influence short episodes of sediment resuspension and transport in the Southwest lagoon of New Caledonia as well as near-bottom circulation and bed shear stress.

After looking at the vertical and directional structure of the currents, we further assessed the seasonal modulation of current and wind intensity (Fig. 5d and 5e, respectively). Wind and current intensity showed a similar seasonal cycle over the 12.5y MOISE observations, with higher intensities during the austral summer and lower intensities during the austral winter. Current intensity median values ranged from 0,05 to 0,08 m s⁻¹, while wind intensity ranged from 4,5 to 7,0 m s⁻¹. The highest current intensities were recorded from January to April, with median values between 0,07 and 0,08 m s⁻¹, associated with median wind intensities between 6,0 and 7,0 m s⁻¹. A marked decrease was observed from May to August, when median current intensity falling to about 0,05 and 0,06 m s⁻¹, approximately 1.3 times lower than during the January-April period associated also with weaker median wind intensities between 5,0 and 6,0 m s⁻¹. From September to December, current intensity increased again, reaching median values of about 0,05-0,07 m s⁻¹ associated with median wind intensities between 5,5 and 7,0 m s⁻¹.

Overall, this long-term current dataset provides a robust characterization of the local hydrodynamic at the MOISE observation site in the Southwest lagoon of New Caledonia.

https://doi.org/10.5194/essd-2026-653
Preprint. Discussion started: 25 September 2026

Open Access Earth System Science Data Discussions

4.2 Impact of an extreme event on hydrodynamics processes : the case of Ruby

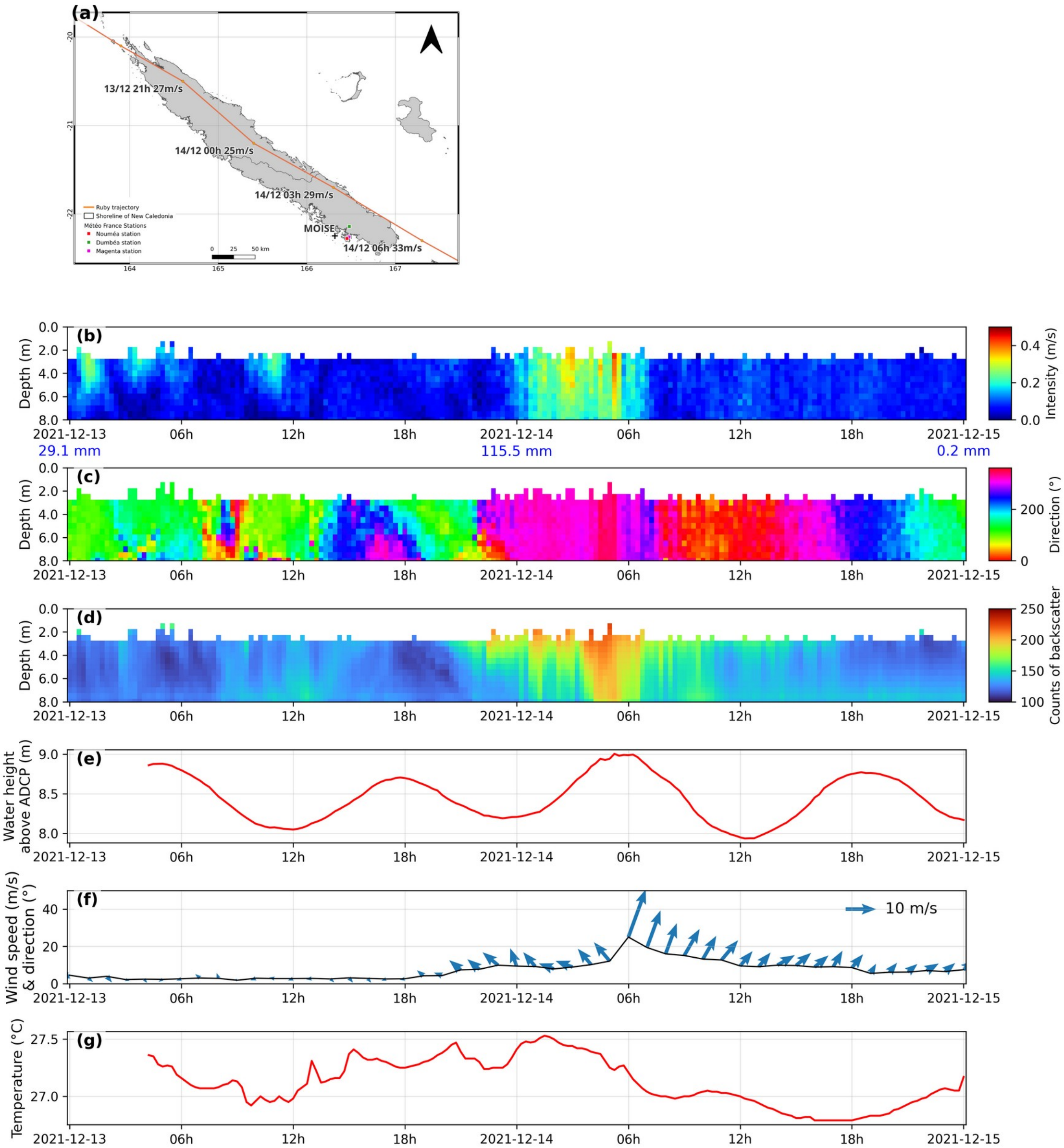

Figure 6: (a) Ruby trajectory, (b) current intensity, (c) current direction, (d) backscatter amplitude, (e) water height above the ADCP derived from ADCP pressure data and atmospheric pressure data, (f) maximum hourly wind speed and direction and (g) temperature from ADCP sensor. Meteorological data were provided by Météo-France. Atmospheric pressure and wind data were obtained from the Magenta station (22,2602 °S, 166.4736 °E) and precipitation data were obtained from the Dumbéa station (22.1328 °S, 166.4811 °E ; Fig. 6A). Rainfall accumulation shown in blue at the bottom in Fig. 6B was calculated for three periods: the day before Ruby passage, the day of its passage, and the day after its passage.

https://doi.org/10.5194/essd-2026-653
Preprint. Discussion started: 25 September 2026

The time resolution of MOISE dataset allowed to study how currents responded to the passage of extreme events such as tropical cyclone. Here, we selected the Ruby Tropical Depression (TD), as a case study because its trajectory crossed the island from northwest to southeast and likely contributed to the marked rainfall accumulation observed in Fig. 7. Ruby crossed the island between 13 and 14 December 2021 (Fig. 6a), reaching Nouméa at ~01:00:00 (UTC) on 14 December 2021.

The passage of Ruby TD induced marked changes in current intensity and direction, water temperature, backscatter intensity at the study site (6b–g). Wind direction (6f) shifted abruptly from West to Northeast, consistent with the trajectory (Fig. 6a) of the depression.

The first clear hydrodynamic response was an abrupt shift in current direction at approximately 10:00:00 (UTC) on December 13th (Fig. 6e), about two hours after wind speed began to increase. This directional change occurred during a low-tide phase, when the corresponding water level was higher than the preceding and following low tides. Current speed increased thereafter reaching a maximum of 0,37 m s^{-1} for approximately three hours at around 18:00:00 (UTC) on December 14th, during a high-tide phase. The corresponding water level was also higher than the adjacent high-tide phases. These observations suggest that the current response to Ruby may also have been modulated by the tidal phase. The decrease in the atmospheric pressure during Ruby's passage (~995 hPa) might have partly contributed to the elevated water levels through the inverse barometer effect (Wunsch and Stammer, 1997).

Before Ruby's passage, currents were predominantly directed toward the east to southeast. During the event, they shifted toward the Northwest and subsequently alternated between northward and southward directions. This post-event variability may reflect an oscillatory adjustment of the lagoon circulation classically found after tropical cyclones.

Rainfall reached 29,1 mm before the TD arrival on site, increased to 115,5 mm during the passage and dropped back to 0,2 mm after the passage of the depression. Water temperature (6g) decreased during the depression passage by nearly 1 °C before rising again during the first hours of the following day, another classical response of the ocean during cyclones (Jullien et al., 2012; Vincent et al., 2012). At the same time, the backscatter signal (6d) showed a pronounced increase, with maximum values coinciding with the peaks of current intensity, suggesting enhanced sediment resuspension caused by strong mixing within the water column and near the seabed.

This case study highlighted how the passage of a tropical depression event can strongly but temporarily disrupt the prevailing circulation pattern at the station. In general, over the entire study period, the strongest currents events resulted from the passage of similar atmospheric disturbances (not shown). This illustrates that continuous monitoring such as that conducted at MOISE allows capturing variability at different time-scales from short-term variability associated with extreme

https://doi.org/10.5194/essd-2026-653
Preprint. Discussion started: 25 September 2026

events, to longer time variability such as seasonal changes in currents (see previous section), offering valuable insights into the circulation dynamics of the south-western lagoon of New Caledonia.

4.3 From temporal dynamics of temperature/salinity to fluorescence/chlorophyll properties at the MOISE station

The MOISE dataset provided observation of temperature, salinity (Fig. 7) and fluorescence-derived chlorophyll quality-controlled profiles (Fig. 8) (see Sect. 4.2.3 : “CTD quality control” for a description of the fluorescence transformation into adjusted fluorescence values).

4.3.1 Long-term variability

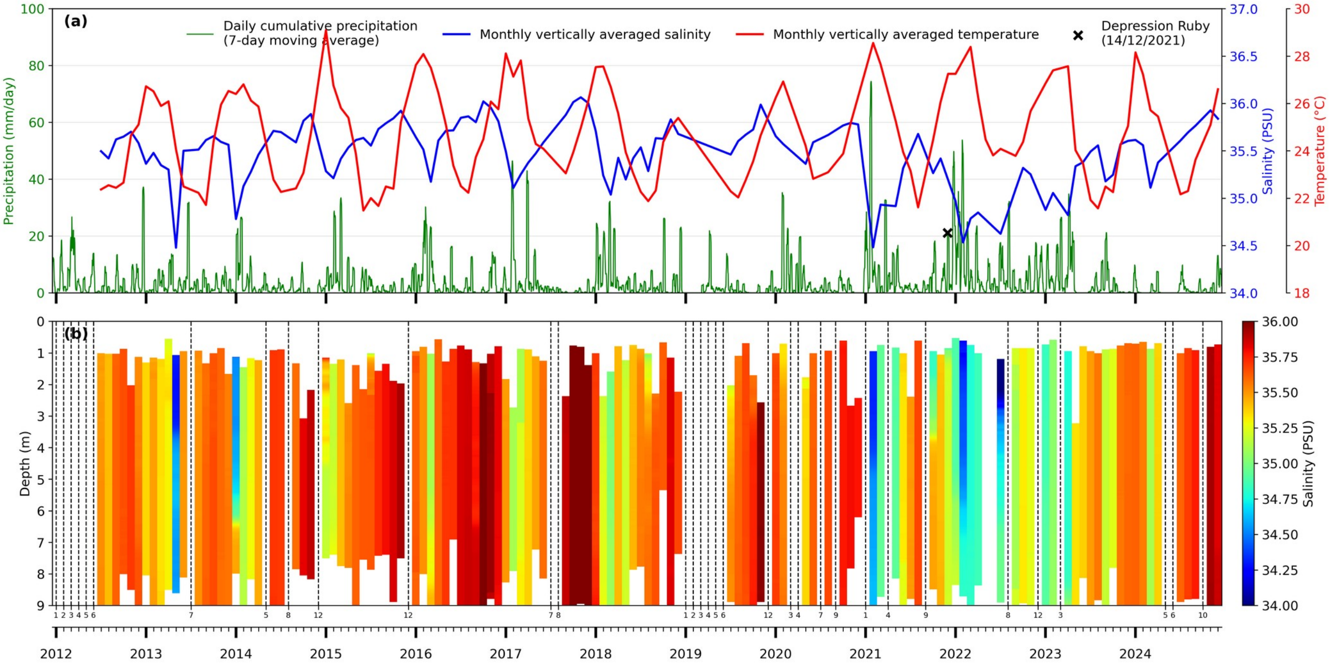

Figure 7: (a) Daily cumulative precipitation (7-day moving average, in green), and vertically- averaged salinity (in blue) and temperature (in red) time series. (b) Monthly vertical profiles of salinity. CTD descent profiles were used and vertical dashed lines indicate months with missing data.

https://doi.org/10.5194/essd-2026-653
Preprint. Discussion started: 25 September 2026

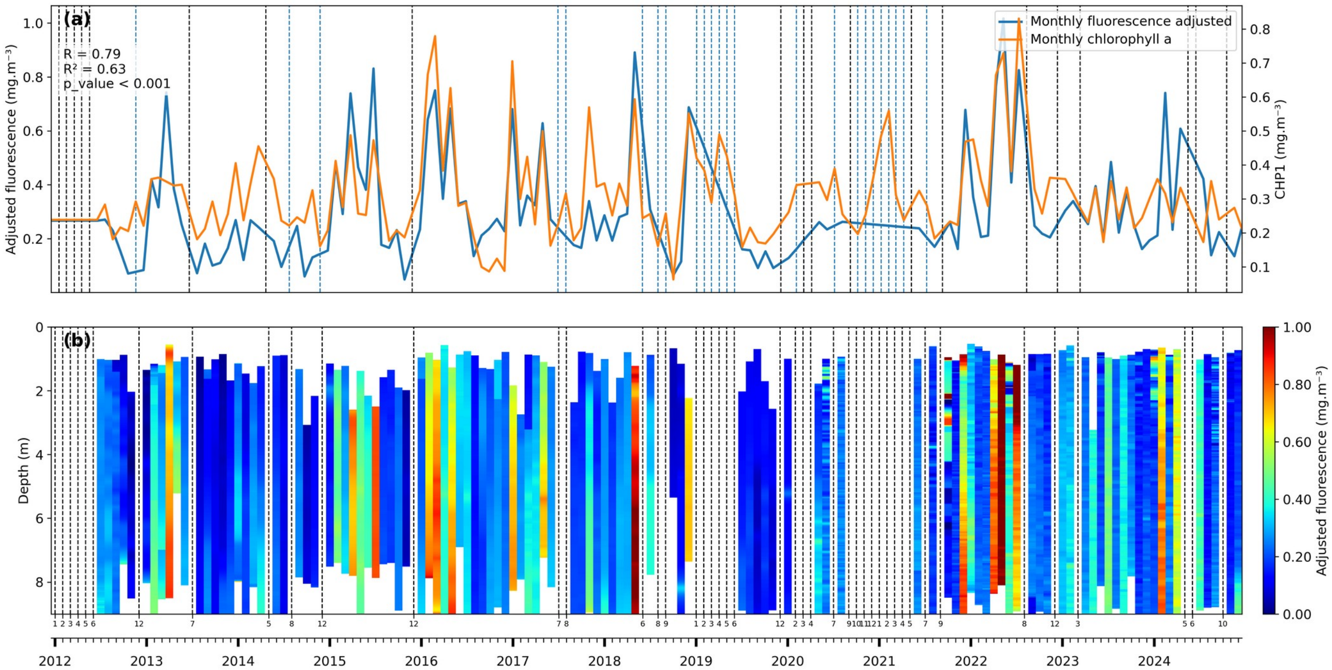

Figure 8: (a) Monthly vertical mean time series of adjusted fluorescence and extracted chlorophyll-a (R=0.79, R^2=0.63,, p-value=0.001 using Pearson statistics and corresponding T-test for p-value) and (b) Monthly vertical profiles of fluorescence. CTD downcast profiles are shown. Vertical dashed lines indicate months with missing data: blue lines represent missing fluorescence data and black lines indicate months where both fluorescence and chlorophyll-a data are missing.

At MOISE, temperature was found to be dominated by seasonal variations, with austral summer maxima and winter minima (red curve, Fig. 7a). Inter annual differences were also observed, with warmer-than-average austral summers in 2015–2016 and again in 2021–2022. However, there was not clear influence of ENSO (see Fig. 2 for ENSO phases) on lagoon temperature unlike what was generally reported in the literature for air temperature (Menkes, 2012) on the regional scale showing weak temperature increases during La Niña and small temperature cooling during El Niño. It is possible that site-specific environmental conditions at MOISE masked the larger scale ENSO signal in air temperature given the small air temperature variations previously reported (e.g., Menkes, 2012).

Seasonal variations of salinity were evident with lower salinity during summer when rainfall was highest and highest salinity during winter when rainfall was lowest (blue and green curves, Fig 7a), as discussed in more details in Sect. 5.3.2. By contrast to temperature, inter-annual variations were apparent with relatively high salinity values observed in 2016 and during an extended period in the second half of 2017, coinciding with low-rainfall conditions (~7 cumulative months without rain) in response to El Niño conditions (see Fig. 2 for ENSO phases) and as reported by Barbero and Moron (2011). In the opposite way, a prolonged freshening period occurred from 2021 to April 2023, with salinity generally ranging between 34 and 35.2. This period coincided with the long lived 2021-2024 La Niña (SOI >1.0 Fig. 2) enhanced rainfall (green curve, Fig

7a), a precipitation pattern typical of La Niña (Barbero and Moron, 2011). The lagoon observed freshening at MOISE likely reflected the enhanced freshwater inputs into the lagoon directly associated with increased rainfall or indirectly associated with rainfall, via enhanced river outflow from the nearby Dumbéa river. Unlike temperature that was found homogeneous in the 0-9m water column during the entire time period (not show), salinity profiles (Fig. 7b) showed episodes of strongly stratified salinity in the upper meters close to the surface. These were visible during freshening episodes related to intense rainfall such as in early 2016, early 2021 and in early 2022 during Ruby. During these episodes, the upper ~3-4 m layer was markely fresher than waters below.

Fluorescence closely followed the same temporal pattern as extracted chlorophyll-a, even if there were differences in peak amplitudes (Fig. 8a). Both variables showed more variable responses than temperature and salinity. Recurrent periods of high concentrations were observed between 2014 and 2017 (up to ~0.8 mg m^{-3}) and again through 2022 (up to 0.7 mg m^{-3}). Episodic high values were also recorded in January 2021, when chlorophyll-a (Fig. 8a, orange) reached ~0.60 mg m^{-3}, nearly twice the long-term mean concentration (~0.31 mg m^{-3}) and in June 2022, when adjusted fluorescence (Fig. 8a, blue) ranged from 0.80 to 1.00 mg m^{-3} and chlorophyll-a from 0.60 to 0.80 mg m^{-3}. These latter peaks may have coincided with the two major rainfall events of that period (Fig. 7a, green curve), with cumulative precipitation of approximately 600 mm and nearly 800 mm, respectively (see monthly precipitation accumulation in Fig. 2). Such increases may reflect enhanced inputs from the Dumbéa River and expansion of its plume , as river plumes in the Southwest lagoon of New Caledonia have been shown to influence gradients of suspended particulate matter, nutrients, and chlorophyll a, with higher values generally observed in small coastal bays than in the open lagoon (Pinazo et al., 2004; Ouillon et al., 2004; Fichez et al., 2010; Drouzy et al., 2019).

Monthly vertical fluorescence profiles (Fig. 8b) indicated generally weak vertical stratification in the water column. Nevertheless, during some periods, as in 2022, fluorescence values were occasionally higher near the bottom than at the surface, a pattern that may be attributed to resuspension of nutrient-rich sediments and/or benthic microalgae from the seabed.

https://doi.org/10.5194/essd-2026-653
Preprint. Discussion started: 25 September 2026

Open Access Earth System Science Data Discussions

4.3.2 Seasonal cycles

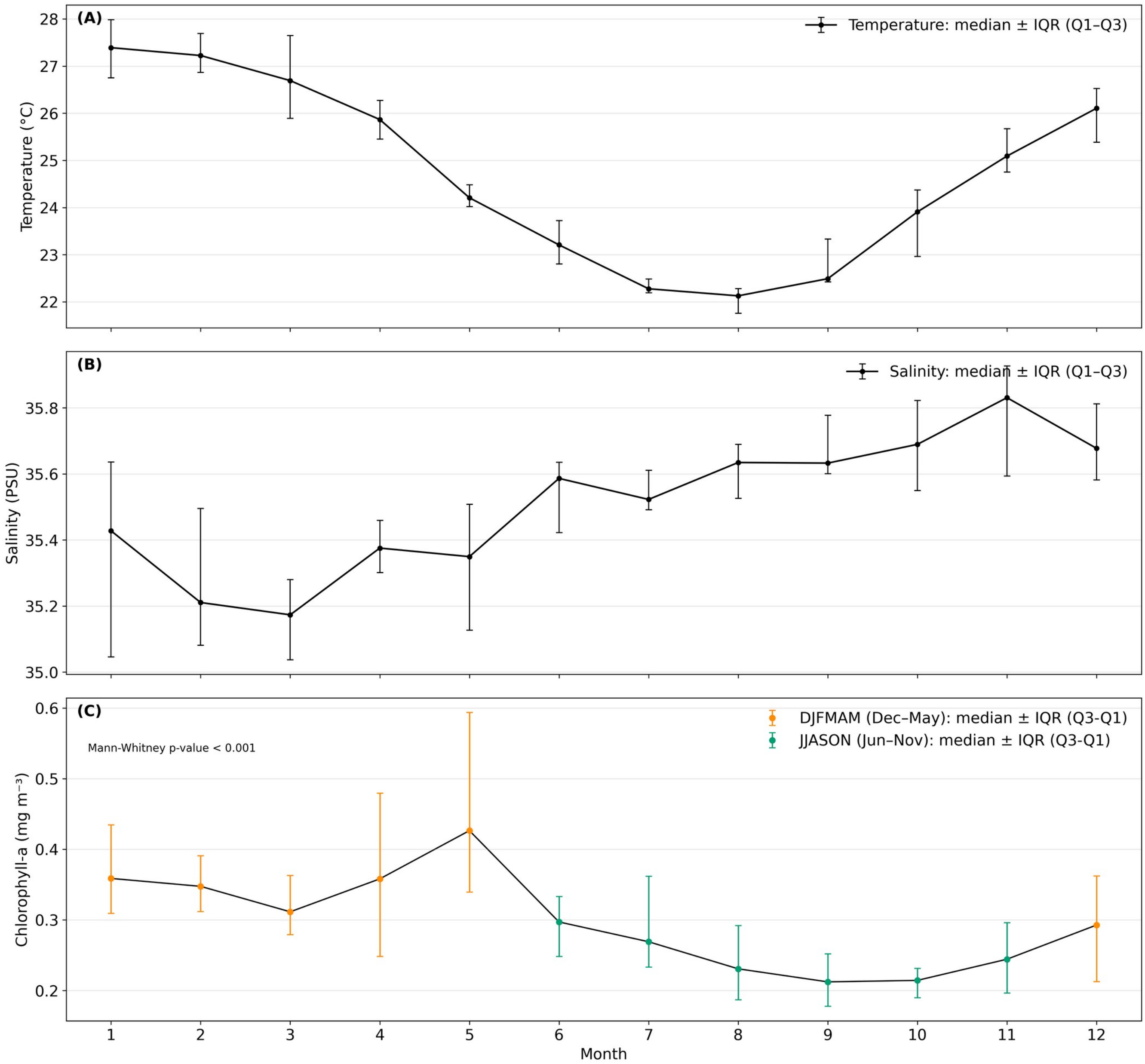

Figure 9: Seasonal cycles of (A) temperature, (B) salinity, and (C) chlorophyll-a at the MOISE station over the 12.5-year observation period. Monthly values are represented by the median, with error bars indicating the interquartile range (Q1–Q3). In panel (C), colors distinguish the two seasonal groups used for the Mann–Whitney test: DJFMAM (December–May) and JJASON (June–November); the corresponding p-value is indicated on the panel.

While inter annual variability at MOISE may be influenced by both large-scale climatic forcing and local episodic processes, the MOISE time series also displayed a clear seasonal variability as evoked above.

Seasonal cycle of temperature and salinity showed opposite variations over the year (Fig. 9A and 9B). Temperature was highest during the austral summer (December-March), then decreased progressively to a minimum during the austral winter (July–August), before increasing again to summer values. In contrast, salinity was lower during summer, increased again in June and reached its highest values during the winter (cooler) season, October and November. Temperature ranged from about 26 to 28 °C in summer to 22 to 24 °C in winter, while salinity tended to be lower in summer (35.1–35.4 PSU) and higher in winter (35.5–35.7 PSU).

Chlorophyll seasonal variability (Fig. 9C) showed relatively high median concentrations from January to May, followed by a progressive decrease from June to September–October, and an increase again in November. A Mann-Whitney test showed a significant (p-value < 0.001) difference between DJFMAM (Dec–May) and JJASON (Jun–Nov) values. The seasonal maximum occurred in May, with median chlorophyll exceeding 0.4 mg m^{-3} and high variability depicted by the interquartile range between 0.3 and 0.6 mg m^{-3}. This variability, also observed in April, may be explained by several mechanisms such as terrigenous inputs (due to rainfall event) , sediment resuspension due to wind or ocean circulation that may have diverted the plume of fresher water from the Dumbéa river, and episodic phytoplankton blooms either from microalgae and small diazotrophs (Saulia et al., 2020) or summer Trichodesmium blooms (Rodier and Le Borgne, 2008).

4.3.3 Summary and potential drivers

Precipitation appeared to be one of the main factors controlling monthly salinity and salinity stratification at the station. Its influence was clearly reflected in the daily precipitation records and monthly salinity time series: when rainfall persisted over several consecutive days, salinity decreased, whereas it increased during dry periods. Part of the observed salinity variability, including the formation of low-salinity surface lenses (Fig. 7B), can therefore be attributed to episodic freshwater inputs following intense rainfall events. Previous studies on New Caledonia watersheds have shown that the hydrological response to rainfall is rapid, with a delay generally shorter than 24 hours between precipitation and freshwater discharge into the lagoon (Domet, 2022).

Among these episodic disturbances, tropical depressions and cyclones certainly played an important role by generating extreme daily precipitation peaks. For instance, Ruby (December 2021) may likely have contributed to one of the major rainfall peaks in the series (Fig. 7A) and may have favored the development of low-salinity conditions at the station. Its influence on phytoplankton dynamics cannot be fully resolved from the monthly sampling alone, but such events are likely to contribute to the short-term anomalies observed in salinity, adjusted fluorescence and chlorophyll-a. Extreme events can induce sharp decreases in salinity, enhanced terrigenous runoff, and marked changes in chlorophyll-a concentrations and microbial communities (Meyneng et al., 2024). For example, Neveux et al (2009) showed that Cyclone Erica (April 2003) associated with strong winds and intense rainfall, had strongly impacted phytoplankton in the Southwestern lagoon, resulting in a 5- to 6-fold increase in surface chlorophyll. Similarly during Cyclone Uesi in February 2020, the discharge of the Dumbéa river increased 40 fold within 24 hours, leading to a 5- to 6-fold rise in surface chlorophyll in the bay that persisted for several days after the cyclone's passage (Meyneng et al., 2024 ; Six et al., 2026). In comparison, the response observed at MOISE after Ruby TD was more moderate (0.5 mg m^{-3}), remaining well below the chlorophyll-a increases reported after strong cyclones or in areas, such as the bay, that are more directly influenced by river discharge, although the single measurement available at MOISE may have missed the peak response.

5 Data availability

The MOISE dataset is publicly available on SEANOE (SEA Scientific Open data Edition) identified by the DOI : https://doi.org/10.17882/98821 (Rodier et al., 2026). Data are open access, provided in NetCDF and CSV format.

6 Conclusion

The MOISE dataset presented in this paper represents the first long-term (12.5 years) multi-parameter monitoring program in the Southwest lagoon of NC, highlighting the links between the atmospheric forcings (e.g. winds, precipitation), hydrodynamics (e.g. currents, temperature, salinity), biogeochemical variability (e.g. chlorophyll, fluorescence, backscatter) over a wide range of time scales such as season, interannual and extreme events such as tropical cyclones.

The observations collected at the MOISE station reveal a climatological pattern, with the dominant circulation mainly oriented toward west-northwest direction, consistent with the influence of the prevailing trade winds. The currents structure of the circulation appears to be controlled by the combined effects of wind forcing, tidal oscillations, bottom friction, and local lagoon geometry.

Current shear increases markedly during extreme events, highlighting the rapid and clear hydrodynamic response of the lagoon to strong atmospheric forcing. Temperature variability is primarily controlled by seasonality, with no clear ENSO-related signal detected at the MOISE station. Salinity appears strongly linked to precipitation, with freshening during wet periods and the formation of low-salinity lenses in the upper water column. Biogeochemical variability, particularly fluorescence and chlorophyll-a, is more episodic, with pronounced peaks observed in 2021-2022 that may be related to terrigenous inputs, runoff and sediment resuspension.

Finally, the MOISE station, located along river mouth provides a key long-term dataset to study land-sea interactions and middle lagoon environmental change driven by climate variability.

All MOISE datasets are openly available at: https://doi.org/10.17882/98821 (Rodier et al., 2026). Those presented in this paper are quality-controlled, and provided in NetCDF and CSV formats, in line with FAIR data principles (Wilkinson et al., 2016).

https://doi.org/10.5194/essd-2026-653
Preprint. Discussion started: 25 September 2026

Appendix A

Table A1 : Downcast and Upcast profile *(Blue : Downcast/Upcast ; Green : Downcast only ; Grey: no data)*

Year **Month**	2012	2013	2014	2015	2016	2017	2018	2019	2020	2021	2022	2023	2024
Jan	Grey	Blue	Blue	Blue	Blue	Blue	Blue	Green	Grey	Grey	Blue	Blue	Blue
Fév	Grey	Blue	Blue	Blue	Blue	Blue	Blue	Green	Green	Blue	Blue	Blue	Blue
Mar	Grey	Blue	Blue	Blue	Blue	Blue	Blue	Green	Grey	Blue	Blue	Grey	Blue
Avr	Grey	Blue	Blue	Blue	Blue	Blue	Blue	Green	Grey	Blue	Blue	Blue	Blue
Mai	Grey	Blue	Grey	Blue	Blue	Blue	Blue	Green	Blue	Grey	Blue	Blue	Grey
Juin	Grey	Blue	Blue	Blue	Blue	Blue	Blue	Grey	Blue	Blue	Blue	Blue	Grey
Juil	Blue	Grey	Blue	Blue	Blue	Grey	Blue	Blue	Grey	Blue	Blue	Blue	Blue
Août	Blue	Blue	Grey	Blue	Blue	Grey	Blue	Blue	Blue	Blue	Grey	Blue	Blue
Sept	Blue	Blue	Blue	Blue	Blue	Blue	Blue	Blue	Grey	Grey	Blue	Blue	Blue
Oct	Blue	Blue	Blue	Blue	Blue	Blue	Blue	Blue	Blue	Blue	Blue	Blue	Grey
Nov	Blue	Blue	Blue	Blue	Blue	Blue	Blue	Blue	Blue	Blue	Blue	Blue	Blue
Déc	Blue	Blue	Grey	Grey	Blue	Blue	Blue	Grey	Blue	Blue	Grey	Grey	Blue

Appendix B

Table B1: Description of the sensors used on CTD probes

Sensors from Sbe19plus CTD profilers (Seabird)	**Parameter**	**Sensor's name**	**Characteristics**
Sensors integrated	Temperature		Range : -5 - +35°C Accuracy : +- 0,005°C
	Conductivity		Range : 0 - 9 S/m Accuracy : +- 0,0005 S/m
	Pressure	Strain-gauge sensor	Various ranges : 20/100/350/600/1000/2000/3500/7000 meters Accuracy : +- 0,1% of full scale range

https://doi.org/10.5194/essd-2026-653
Preprint. Discussion started: 25 September 2026

External sensors	Fluorescence	Wetlabs ECO-FL	Wavelength : 460/695 nm Sensitivity : 0.03 µg/l Range,typical : 0.03–75 µg/l
	Fluorescence and Turbidity	WET Labs ECO-AFL/FL	**Turbidity** Wavelength : 700 nm Sensitivity : 0.01 NTU Range : 0-25 NTU **Fluorescence** Wavelength : 470/695 nm Sensitivity : 0.0025 µg/l Range : 0-50 µg/l
	Turbidity	Upoly 0 (zéro order polynomial calibration)	
	Turbidity	Seapoint	Wavelength : 880 nm Sensitivity : 2 mV/FTU Range : 0-4000 FTU
	Irradiance/PAR	Biospherical/Licor (QSP-2000)	Sensitivity : 1×10^{17}quanta/(cm²·s) Dynamic range : $1{,}4 \times 10^{-5}$ µE/(cm²·s) à 0,5 µE/(cm²·s)
	PH	SBE18	Range : 0 - 14 Accuracy : +- 0.1

Appendix C

Table C1 : Sensor-specific linear regression coefficients and associated statistical metrics (R^2 and p-value) for fluorescence calibrations.

Serial number, sensor name, calibration date	**Linear regression coefficient (a,b)**	**R^2**	**p_value**
"4861", "WET Labs ECO-AFL/FL", "2011-04-28"	1.17, 0.37	0.23	0.0057
"7973", "WET Labs ECO-AFL/FL", "2019-05-30"	0.29, 0.10	0.95	0.0234
"4861", "WET Labs ECO-AFL/FL", "2021-09-17"	0.65, 0.02	0.79	0.0000
"4310", "WET Labs ECO-AFL/FL", "2020-11-19"	0.43, 0.05	0.39	0.0000
"4310", "WET Labs WETstar", "2012-04-10"	0.72, 0.07	0.47	0.0000
"4310", "WET Labs WETstar", "2020-11-19"	-1.82, 0.36	0.22	0.5363
"6277", "WET Labs ECO-AFL/FL", "2017-06-11"	-0.09, 0.20	0.01	0.8900
"4861", "WET Labs ECO-AFL/FL", "2016-09-05"	0.01, 0.18	0.00	0.9525

https://doi.org/10.5194/essd-2026-653
Preprint. Discussion started: 25 September 2026

Table C2 : ratio R, calculated as fluorescence divided by chlorophyll-a concentration.

Date	**Cast**	**serial_number_profiler / sensor_name/ calibration_date**	**Ratio R**
2020-12-10	01	4861 — WET Labs ECO-AFL/FL — 2016-09-05	2.148
2020-10-01	01	4861 — WET Labs ECO-AFL/FL — 2016-09-05	0.957
2021-02-16	01	4861 — WET Labs ECO-AFL/FL — 2016-09-05	3.155
2020-06-21	02	6277 — WET Labs ECO-AFL/FL — 2017-06-11	1.737
2020-08-24	01	7973 — WET Labs ECO-AFL/FL — 2019-05-30	1.344
2021-02-16	01	4861 — WET Labs ECO-AFL/FL — 2016-09-05	3.335
2020-11-23	01	4861 — WET Labs ECO-AFL/FL — 2016-09-05	0.974
2020-06-21	02	6277 — WET Labs ECO-AFL/FL — 2017-06-11	1.834
2020-05-11	02	7973 — WET Labs ECO-AFL/FL — 2019-05-30	0.816
2020-10-01	01	4861 — WET Labs ECO-AFL/FL — 2016-09-05	0.931
2021-07-26	01	4310 — WET Labs WETstar — 2020-11-19	2.698
2021-06-28	02	4310 — WET Labs WETstar — 2020-11-19	1.620
2020-10-29	01	4861 — WET Labs ECO-AFL/FL — 2016-09-05	1.477
2020-08-24	02	6277 — WET Labs ECO-AFL/FL — 2017-06-11	1.316
2020-10-29	01	4861 — WET Labs ECO-AFL/FL — 2016-09-05	1.464
2021-03-01	01	4861 — WET Labs ECO-AFL/FL — 2016-09-05	1.572
2021-07-26	01	4310 — WET Labs WETstar — 2020-11-19	2.696
2021-03-01	01	4861 — WET Labs ECO-AFL/FL — 2016-09-05	1.600
2020-05-11	03	7973 — WET Labs ECO-AFL/FL — 2019-05-30	0.879
2020-08-24	02	6277 — WET Labs ECO-AFL/FL — 2017-06-11	1.386
2020-05-11	02	7973 — WET Labs ECO-AFL/FL — 2019-05-30	0.894
2020-11-23	01	4861 — WET Labs ECO-AFL/FL — 2016-09-05	1.197
2020-12-10	01	4861 — WET Labs ECO-AFL/FL — 2016-09-05	2.146
2020-08-24	01	7973 — WET Labs ECO-AFL/FL — 2019-05-30	1.507
2021-06-28	02	4310 — WET Labs WETstar — 2020-11-19	1.459
2020-05-11	03	7973 — WET Labs ECO-AFL/FL — 2019-05-30	0.870

Appendix D

Table D1 : Quality code description based on NERC Vocabulary Server (NVS), RD2 Argo delayed-mode quality control measurement flags http://vocab.nerc.ac.uk/collection/RD2/current/

CODE	**LABEL**	**QUALITY**
0	No quality control has been performed on this	No QC

https://doi.org/10.5194/essd-2026-653
Preprint. Discussion started: 25 September 2026

	element	
1	The element appears to be correct	Good data
2	The element appears to be probably good	"Probably" good data
3	The element appears doubtful	"Probably" bad data
4	The element appears erroneous	Bad data
5	The element has been changed	Changed
6	Reserved for future use	Additional qualification
7	Reserved for future use	Reserved
8	Reserved for future use	Reserved
9	The element is missing	Element missing

Appendix E

Table E1 : Processing state description based on NERC Vocabulary Server (NVS) R06 (https://vocab.nerc.ac.uk/collection/R06/current/).

CODE	**LABEL**	**DEFINITION**
0A	RAW DATA	Data are the raw output from instruments, without calibration, and not necessarily converted to engineering units (Level 0).
0B	AUTOMATIC QUALITY CONTROL	
0C	VISUAL CHECK	
1A	CLIMATOLOGY CONTROL	Data have been converted to values independent of detailed instrument knowledge; automated calibrations may have been done; data may not have full geospatial and temporal referencing, but have sufficient information to uniquely reference the data to the point

https://doi.org/10.5194/essd-2026-653
Preprint. Discussion started: 25 September 2026

		of measurement (Level 1).
1B	APPLICATION OF QUALITY CODE AFTER VISUAL INSPECTION	
1C	VALIDED BY PI	
2A	NOT RECOMMEND	
2B	NOT RECOMMEND	Data have complete geospatial and temporal references; information may have been sub-sampled, averaged or compressed in other ways, but no assumptions of scales and variability or thermodynamic relationships have been used in the processing (Level 2).
2B+	CALIBRATED DATA	Data have complete geospatial and temporal references; information may have been sub-sampled, averaged or compressed in other ways, but no assumptions of scales and variability or thermodynamic relationships have been used in the processing (Level 2).
2C	NOT RECOMMEND	Data have complete geospatial and temporal references; information may have been sub-sampled, averaged or compressed in other ways, but no assumptions of scales and variability or thermodynamic relationships have been used in the processing (Level 2).
2C+	CALIBRATED DATA VALIDATED BY PI	Data have complete geospatial and temporal references; information may have been sub-sampled, averaged or compressed in other ways, but no assumptions of scales and variability or thermodynamic relationships have been used in the processing (Level 2). In addition, the data are fully quality controlled and peer-reviewed, and are widely accepted as valid; documentation is complete and widely available.
3B	CALIBRATED REDUCED DATA	Data have been processed with assumptions about the scales of variability or thermodynamic relationships; the data are normally reduced to regular space, time intervals with enhanced signal to noise (Level 3).

https://doi.org/10.5194/essd-2026-653
Preprint. Discussion started: 25 September 2026

3C	GRIDDED REDUCED DATA	Data have been processed with assumptions about the scales of variability or thermodynamic relationships; the data are normally reduced to regular space, time intervals with enhanced signal to noise (Level 3).

650 **Appendix F**

Table F1 : ADCP variables and associated descriptions

Variable	**Description**	**Units**
EWCT	Eastward component	meter per second
NSCT	Northward component	meter per second
UVCT	Upward component	meter per second
HEAD	Heading	degree
PITCH	Pitch	degree
ROLL	Roll	degree
PRES	Pressure	dbar
TEMP	Temperature	degree Celsius
SAMA	Backscatter amplitude	counts

Table F2 : CTD variables and associated descriptions

Variable	**Description**	**Units**
CNDC	Conductivity	siemens per meter
FLU2	Fluorescence	milligram per cubic meter
LGHT	Irradiance	microeinsteins per square meter per second

https://doi.org/10.5194/essd-2026-653
Preprint. Discussion started: 25 September 2026

PHPH	pH	
PRES	Pressure	dbar
TEMP	Temperature	degree Celsius
PSAL	Salinity	PSU
TUR4	Turbidity	NTU

655 Table F3 : Description of the variable associated to the physical parameters measured from Copernicus Marine In Situ NetCDF Format Manual (section 3.5 ; https://doi.org/10.13155/59938)

Variable	**Description**
PARAM	raw data
PARAM_QC	the quality control flags on PARAM values
PARAM_DM	the data mode of PARAM values
PARAM_UNCERTAINTY	the uncertainty on PARAM values
PARAM_ADJUSTED	the adjusted value of the parameter, usually the delayed-mode adjustment
PARAM_ADJUSTED_ERROR	the error associated to the adjusted parameter
PARAM_ADJUSTED_QC	the QC flag associated to the adjusted parameter

Appendix G

https://doi.org/10.5194/essd-2026-653
Preprint. Discussion started: 25 September 2026

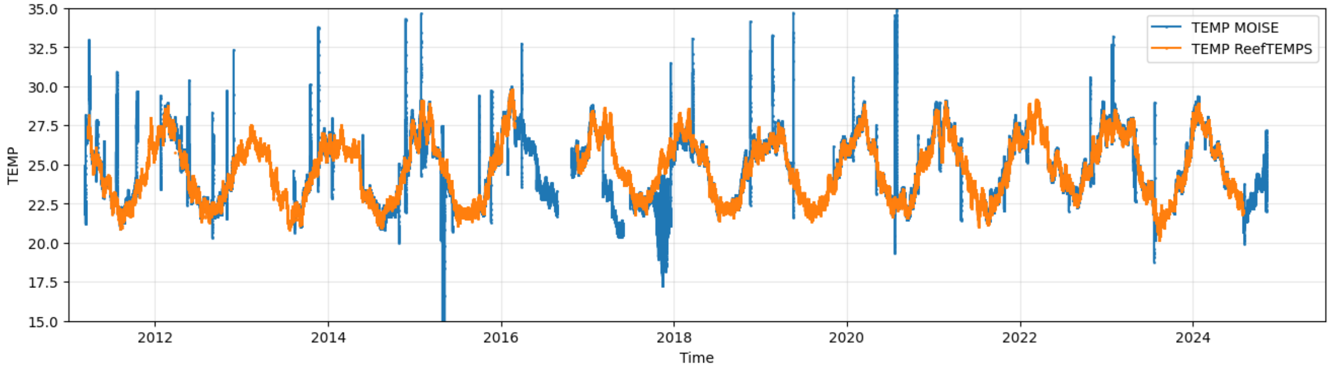

Figure G1 : Raw ADCP temperature data in blue versus temperature data from BAKAUI01 Station from ReefTEMPS in orange.

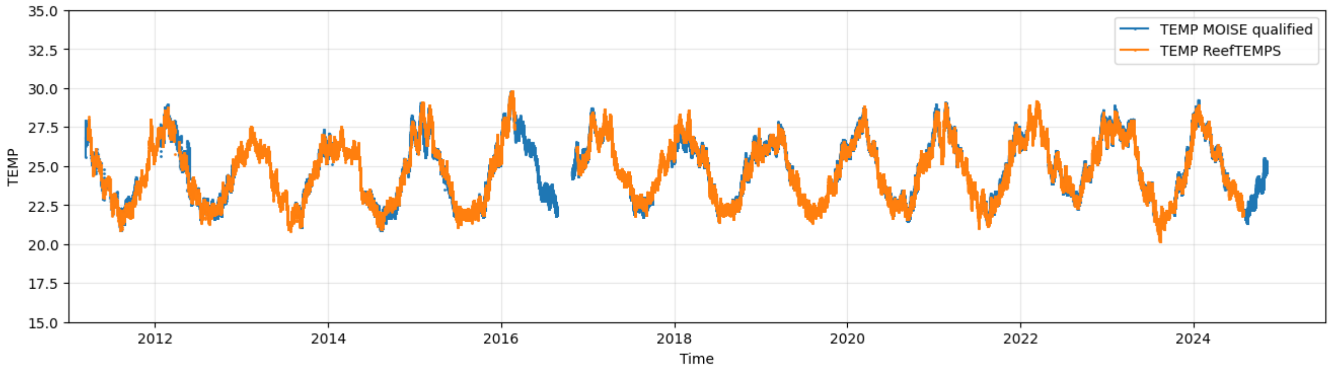

Figure G2 : Validated ADCP temperature data in blue versus temperature data from BAKAUI01 Station from ReefTEMPS in orange.

Author contributions

MR and CD are the Principal Investigators (PIs) of the MOISE Project and were responsible for raising the funds, administrative responsibility.

GP, CD, AD's, EG, VD, CB, DG and AJ carried out the field experiments.

AD's and all members of the LAMA team carried out the analysis of the water samples.

SD, CD, MR, VD, CB, DG, AJ, VD, and CQ organized, processed, checked, and archived the dataset.

SD prepared the original draft of the manuscript.

SD, MR, CD, CM, SF, MD, and CQ contributed to writing, revision, and editing the paper.

https://doi.org/10.5194/essd-2026-653
Preprint. Discussion started: 25 September 2026

CM, SF, CQ, CD, and MR carried out, supervised and coordinated the main author work as Civic Service Volunteering (VSC).

For details about the authors, contributors, and affiliated organizations involved in MOISE, refer to the dataset description on SEANOE: https://doi.org/10.17882/98821 (Rodier et al., 2026).

Acknowledgements

The authors gratefully acknowledge the financial, technical, and logistical support provided throughout the MOISE monitoring program. The instrumentation was supported by MIO and the UAR IMAGO team in Nouméa.
We are grateful to the divers involved in field operations, EE, BB, and DM, and to the captains of the vessels used throughout the monitoring period, TS, CM, NP, GJ, and MN.

We also thank IRD at Nouméa, UMR ENTROPIE and LAMA, the chemistry laboratory of the IRD Center in Nouméa, for carrying out the chemical analyses.

Since 2014, several complementary research projects have contributed to the MOISE monitoring program, including VAHINE (LEFE), TRICHOTOX, TREMOLO (EC2CO), DYNAMINE (CNRT), and TREMOR.

Financial support

MIO research project, OSU Pytheas and IRD Nouméa.

References

Alber, M., Reed, D., and McGlathery, K.: Coastal Long Term Ecological Research: Introduction to the Special Issue, Oceanography, 26, 14–17, https://doi.org/10.5670/oceanog.2013.40, 2013.

Andréfouët, S., Cabioch, G., Flamand, B., and Pelletier, B.: A reappraisal of the diversity of geomorphological and genetic processes of New Caledonian coral reefs: a synthesis from optical remote sensing, coring and acoustic multibeam observations, Coral Reefs, 28, 691–707, https://doi.org/10.1007/s00338-009-0503-y, 2009.

Barbero, R. and Moron, V.: Seasonal to decadal modulation of the impact of El Niño–Southern Oscillation on New Caledonia (SW Pacific) rainfall (1950–2010), Journal of Geophysical Research: Atmospheres, 116, https://doi.org/10.1029/2011JD016577, 2011.

Bindoff, N. L., Cheung, W. W. L., Kairo, J. G., Arístegui, J., Guinder, V. A., Hallberg, R., Hilmi, N., Jiao, N., Karim, M. S., Levin, L., O'Donoghue, S., Purca Cuicapusa, S. R., Rinkevich, B., Suga, T., Tagliabue, A., Williamson, P., Pörtner, H.-O., Roberts, D. C., Masson-Delmotte, V., Zhai, P., Tignor, M., Poloczanska, E., Mintenbeck, K., Alegría, A., Nicolai, M., Okem, A., Petzold, J., Rama, B., and Weyer, N. M.: Changing Ocean, Marine Ecosystems, and Dependent Communities, in: IPCC Special Report on the Ocean and Cryosphere in a Changing Climate, edited by: Pörtner, H.-O., Roberts, D. C., Masson-Delmotte, V., Zhai, P., Tignor, M., Poloczanska, E., Mintenbeck, K., Alegría, A., Nicolai, M., Okem, A., Petzold, J., Rama, B., and Weyer, N. M., Cambridge University Press, Cambridge, UK and New York, NY, USA, 447–587, https://doi.org/10.1017/9781009157964.007, 2019.

Blázquez-García, A., Conde, A., Mori, U., and Lozano, J. A.: A Review on Outlier/Anomaly Detection in Time Series Data, ACM Comput. Surv., 54, 56:1-56:33, https://doi.org/10.1145/3444690, 2021.

Bonvallot, J., Gay, J.-C., and Habert, E.: Atlas de la Nouvelle Calédonie, Marseille et Nouméa, 2012.

Bruyère, O., Soulard, B., Lemonnier, H., Laugier, T., Hubert, M., Petton, S., Desclaux, T., Van Wynsberge, S., Le Tesson, E., Lefèvre, J., Dumas, F., Kayara, J.-F., Bourassin, E., Lalau, N., Antypas, F., and Le Gendre, R.: Hydrodynamic and hydrological processes within a variety of coral reef lagoons: field observations during six cyclonic seasons in New Caledonia, Earth System Science Data, 14, 5439–5462, https://doi.org/10.5194/essd-14-5439-2022, 2022.

Bruyère, O., Le Gendre, R., Chauveau, M., Bourgeois, B., Varillon, D., Butscher, J., Trophime, T., Follin, Y., Aucan, J., Liao, V., and Andréfouët, S.: Lagoon hydrodynamics of pearl farming atolls: the case of Raroia, Takapoto, Apataki and Takaroa (French Polynesia), Earth System Science Data, 15, 5553–5573, https://doi.org/10.5194/essd-15-5553-2023, 2023.

Ceccarelli, D. M., McKinnon, A. D., Andréfouët, S., Allain, V., Young, J., Gledhill, D. C., Flynn, A., Bax, N. J., Beaman, R., Borsa, P., Brinkman, R., Bustamante, R. H., Campbell, R., Cappo, M., Cravatte, S., D'Agata, S., Dichmont, C. M., Dunstan, P. K., Dupouy, C., Edgar, G., Farman, R., Furnas, M., Garrigue, C., Hutton, T., Kulbicki, M., Letourneur, Y., Lindsay, D., Menkes, C., Mouillot, D., Parravicini, V., Payri, C., Pelletier, B., Richer de Forges, B., Ridgway, K., Rodier, M., Samadi, S., Schoeman, D., Skewes, T., Swearer, S., Vigliola, L., Wantiez, L., Williams, A., Williams, A., Richardson, A. J., and Lesser, M.: Chapter Four - The Coral Sea: Physical Environment, Ecosystem Status and Biodiversity Assets, in: Advances in Marine Biology, vol. 66, edited by: Lesser, M., Academic Press, 213–290, https://doi.org/10.1016/B978-0-12-408096-6.00004-3, 2013.

Chancerelle, Y., Sasal, P., Siu, G., and Planes, S.: Importance of long-term surveys to monitor ecosystems: the case study of coral reefs in the South Pacific, One Ocean Science Congress 2025, Nice, France, 3–6 Jun 2025, OOS2025-1520, https://doi.org/10.5194/oos2025-1520, 2025.

Cocquempot, L., Delacourt, C., Paillet, J., Riou, P., Aucan, J., Castelle, B., Charria, G., Claudet, J., Conan, P., Coppola, L., Hocdé, R., Planes, S., Raimbault, P., Savoye, N., Testut, L., and Vuillemin, R.: Coastal Ocean and Nearshore Observation: A French Case Study, Front. Mar. Sci., 6, https://doi.org/10.3389/fmars.2019.00324, 2019.

Desclaux, T., Lemonnier, H., Genthon, P., Soulard, B., and Le Gendre, R.: Suitability of a lumped rainfall–runoff model for flashy tropical watersheds in New Caledonia, Hydrological Sciences Journal, 63, 1689–1706, https://doi.org/10.1080/02626667.2018.1523613, 2018.

Doblas-Reyes, F. J., Sörensson, A. A., Almazroui, M., Dosio, A., Gutowski, W. J., Haarsma, R., Hamdi, R., Hewitson, B., Kwon, W.-T., Lamptey, B. L., Maraun, D., Stephenson, T. S., Takayabu, I., Terray, L., Turner, A., Zuo, Z., Masson-Delmotte, V., Zhai, P., Pirani, A., Connors, S. L., Péan, C., Berger, S., Caud, N., Chen, Y., Goldfarb, L., Gomis, M. I., Huang, M., Leitzell, K., Lonnoy, E., Matthews, J. B. R., Maycock, T. K., Waterfield, T., Yelekçi, O., Yu, R., and Zhou, B.: Linking Global to Regional Climate Change, in: Climate Change 2021: The Physical Science Basis, edited by: Masson-Delmotte, V., Zhai, P., Pirani, A., Connors, S. L., Péan, C., Berger, S., Caud, N., Chen, Y., Goldfarb, L., Gomis, M. I., Huang, M., Leitzell, K., Lonnoy, E., Matthews, J. B. R., Maycock, T. K., Waterfield, T., Yelekçi, O., Yu, R., and Zhou, B., Cambridge University Press, Cambridge, United Kingdom and New York, NY, USA, 1363–1512, https://doi.org/10.1017/9781009157896.012, 2021.

Domet, M.-A.: Recueil des débits caractéristiques de la Nouvelle-Calédonie - Actualisation jusqu'à la période 2019/2021, DAVAR-SDE, Nouvelle Calédonie, 2022.

Douillet, P.: Tidal dynamics of the south-west lagoon of New Caledonia: observations and 2D numerical modelling, Oceanologica Acta, 21, 69–79, https://doi.org/10.1016/S0399-1784(98)80050-9, 1998.

Douillet, P., Ouillon, S., and Cordier, E.: A numerical model for fine suspended sediment transport in the Southwest lagoon of New Caledonia, Coral Reefs, 20, 361–372, https://doi.org/10.1007/s00338-001-0193-6, 2001.

Dumas, F., Le Gendre, R., Thomas, Y., and Andréfouët, S.: Tidal flushing and wind driven circulation of Ahe atoll lagoon (Tuamotu Archipelago, French Polynesia) from in situ observations and numerical modelling, Marine Pollution Bulletin, 65, 425–440, https://doi.org/10.1016/j.marpolbul.2012.05.041, 2012.

Duphil, M., Lefèvre, J., Jullien, S., Roger, J., Dumas, P., Le Gendre, R., Aucan, J., Vendé-Leclerc, M., Bénébig, M., and Menkes, C.: The role of barrier reef protection to storm surge during tropical cyclones in a narrow lagoon, New Caledonia, south west Pacific, Continental Shelf Research, 294, 105540, https://doi.org/10.1016/j.csr.2025.105540, 2025.

Dupouy, C., Neveux, J., Ouillon, S., Frouin, R., Murakami, H., Hochard, S., and Dirberg, G.: Inherent optical properties and satellite retrieval of chlorophyll concentration in the lagoon and open ocean waters of New Caledonia, Marine Pollution Bulletin, 61, 503–518, https://doi.org/10.1016/j.marpolbul.2010.06.039, 2010.

Dupouy, C., Whiteside, A., Tan, J., Wattelez, G., Murakami, H., Andréoli, R., Lefèvre, J., Röttgers, R., Singh, A., and Frouin, R.: A Review of Ocean Color Algorithms to Detect Trichodesmium Oceanic Blooms and Quantify Chlorophyll Concentration in Shallow Coral Lagoons of South Pacific Archipelagos, Remote Sensing, 15, https://doi.org/10.3390/rs15215194, 2023.

Dupouy, C. and Rodier, M.: MOISE : MOuillage Instrumenté et Suivi biogEochimique du lagon sud-ouest de la Nouvelle-Calédonie (2012-2024), IRD - Institut de recherche pour le développement, Nouméa, https://doi.org/10.23708/fdi:010096702, 2026.

Dutheil, C., Menkes, C., Lengaigne, M., Vialard, J., Peltier, A., Bador, M., and Petit, X.: Fine-scale rainfall over New Caledonia under climate change, Clim Dyn, 56, 87–108, https://doi.org/10.1007/s00382-020-05467-0, 2021.

https://doi.org/10.5194/essd-2026-653
Preprint. Discussion started: 25 September 2026

Fichez, R., Chifflet, S., Douillet, P., Gérard, P., Gutierrez, F., Jouon, A., Ouillon, S., and Grenz, C.: Biogeochemical typology and temporal variability of lagoon waters in a coral reef ecosystem subject to terrigeneous and anthropogenic inputs (New Caledonia), Marine Pollution Bulletin, 61, 309–322, https://doi.org/10.1016/j.marpolbul.2010.06.021, 2010.

Fox-Kemper, B., Hewitt, H. T., Xiao, C., Aðalgeirsdóttir, G., Drijfhout, S. S., Edwards, T. L., Golledge, N. R., Hemer, M., Kopp, R. E., Krinner, G., Mix, A., Notz, D., Nowicki, S., Nurhati, I. S., Ruiz, L., Sallée, J.-B., Slangen, A. B. A., Yu, Y., Masson-Delmotte, V., Zhai, P., Pirani, A., Connors, S. L., Péan, C., Berger, S., Caud, N., Chen, Y., Goldfarb, L., Gomis, M. I., Huang, M., Leitzell, K., Lonnoy, E., Matthews, J. B. R., Maycock, T. K., Waterfield, T., Yelekçi, O., Yu, R., and Zhou, B.: Ocean, Cryosphere and Sea Level Change, in: Climate Change 2021: The Physical Science Basis, edited by: Masson-Delmotte, V., Zhai, P., Pirani, A., Connors, S. L., Péan, C., Berger, S., Caud, N., Chen, Y., Goldfarb, L., Gomis, M. I., Huang, M., Leitzell, K., Lonnoy, E., Matthews, J. B. R., Maycock, T. K., Waterfield, T., Yelekçi, O., Yu, R., and Zhou, B., Cambridge University Press, Cambridge, United Kingdom and New York, NY, USA, 1211–1362, https://doi.org/10.1017/9781009157896.011, 2021.

Grenz, C., Le Borgne, R., Fichez, R., and Torréton, J.-P.: Tropical lagoon multidisciplinary investigations: An overview of the PNEC New Caledonia pilot site, Marine Pollution Bulletin, 61, 267–268, https://doi.org/10.1016/j.marpolbul.2010.06.030, 2010.

Johnson, J. E. and Wabnitz, C. C. C. (Eds.): Climate change implications for fisheries and aquaculture in the Pacific Islands region, Noumea, New Caledonia, 626 pp., 2025.

Jullien, S., Menkes, C. E., Marchesiello, P., Jourdain, N. C., Lengaigne, M., Koch-Larrouy, A., Lefèvre, J., Vincent, E. M., and Faure, V.: Impact of Tropical Cyclones on the Heat Budget of the South Pacific Ocean, Journal of Physical Oceanography, 42, 1882–1906, https://doi.org/10.1175/JPO-D-11-0133.1, 2012.

Le Gendre, R., Varillon, D., Fiat, S., Hocdé, R., de Ramon N'Yeurt, A., Andréfouët, S., Aucan, J., Cravatte, S., Duphil, M., Ganachaud, A., Gaudron, B., Kestenare, E., Liao, V., Pelletier, B., Peltier, A., Schaefer, A.-L., Trophime, T., Van Wynsberge, S., Dandonneau, Y., Allenbach, M., and Menkes, C.: ReefTEMPS: the Pacific Islands coastal temperature network, Earth System Science Data, 17, 5277–5301, https://doi.org/10.5194/essd-17-5277-2025, 2025.

Lefèvre, J., Marchesiello, P., Jourdain, N. C., Menkes, C., and Leroy, A.: Weather regimes and orographic circulation around New Caledonia, Marine Pollution Bulletin, 61, 413–431, https://doi.org/10.1016/j.marpolbul.2010.06.012, 2010.

Leichter, J. J., Stokes, M. D., Hench, J. L., Witting, J., and Washburn, L.: The island-scale internal wave climate of Moorea, French Polynesia, Journal of Geophysical Research: Oceans, 117, https://doi.org/10.1029/2012JC007949, 2012.

Leichter, J. J., Alldredge, A. L., Bernardi, G., Brooks, A. J., Carlson, C. A., Carpenter, R. C., Edmunds, P. J., Fewings, M. R., Hanson, K. M., Hench, J. L., Holbrook, S. J., Nelson, C. E., Schmitt, R. J., Toonen, R. J., Washburn, L., and Wyatt, A. S. J.: Biological and Physical Interactions on a Tropical Island Coral Reef: Transport and Retention Processes on Moorea, French Polynesia, Oceanography, 26, 52–63, https://doi.org/10.5670/oceanog.2013.45, 2013.

https://doi.org/10.5194/essd-2026-653
Preprint. Discussion started: 25 September 2026

Leys, C., Ley, C., Klein, O., Bernard, P., and Licata, L.: Detecting outliers: Do not use standard deviation around the mean, use absolute deviation around the median, Journal of Experimental Social Psychology, 49, 764–766, https://doi.org/10.1016/j.jesp.2013.03.013, 2013.

Martias, C.: Dynamique de la matière organique dissoute colorée et fluorescente en zone lagonaire tropicale dans le Pacifique Sud (Nouvelle-Calédonie) : influences climatiques et anthropogéniques, Ph.D. thesis, Aix-Marseille Université, Marseille, France, 2018.

Menkès, C.: Les grandes fluctuations des hydroclimats : le phénomène ENSO, in: Atlas de la Nouvelle-Calédonie, edited by: Bonvallot, J., Gay, J.-C., and Habert, E., IRD, Congrès de la Nouvelle-Calédonie, Marseille, France, and Nouméa, New Caledonia, 49–52, ISBN 978-2-7099-1740-1, 2012.

Meyneng, M., Lemonnier, H., Le Gendre, R., Plougoulen, G., Antypas, F., Ansquer, D., Serghine, J., Schmitt, S., and Siano, R.: Subtropical coastal microbiome variations due to massive river runoff after a cyclonic event, Environmental Microbiome, 19, 10, https://doi.org/10.1186/s40793-024-00554-9, 2024.

Moron, V., Barbero, R., and Robertson, A. W.: Subseasonal-to-interannual variability of rainfall over New Caledonia (SW Pacific), Clim Dyn, 46, 2449–2468, https://doi.org/10.1007/s00382-015-2712-0, 2016.

Neveux, J., Tenório, M. M. B., Jacquet, S., Torréton, J.-P., Douillet, P., Ouillon, S., and Dupouy, C.: Chlorophylls and Phycoerythrins as Markers of Environmental Forcings Including Cyclone Erica Effect (March 2003) on Phytoplankton in the Southwest Lagoon of New Caledonia and Oceanic Adjacent Area, International Journal of Oceanography, 2009, 232513, https://doi.org/10.1155/2009/232513, 2009.

Ouillon, S., Douillet, P., Fichez, R., and Panché, J.-Y.: Enhancement of regional variations in salinity and temperature in a coral reef lagoon, New Caledonia, Comptes Rendus Geoscience, 337, 1509–1517, https://doi.org/10.1016/j.crte.2005.08.005, 2005.

Ouillon, S., Douillet, P., Lefebvre, J. P., Le Gendre, R., Jouon, A., Bonneton, P., Fernandez, J. M., Chevillon, C., Magand, O., Lefèvre, J., Le Hir, P., Laganier, R., Dumas, F., Marchesiello, P., Bel Madani, A., Andréfouët, S., Panché, J. Y., and Fichez, R.: Circulation and suspended sediment transport in a coral reef lagoon: The south-west lagoon of New Caledonia, Marine Pollution Bulletin, 61, 269–296, https://doi.org/10.1016/j.marpolbul.2010.06.023, 2010.

Pagli, B., Duphil, M., Jullien, S., Dutheil, C., Peltier, A., and Menkes, C.: Wave climate around New Caledonia, Clim Dyn, 62, 8865–8887, https://doi.org/10.1007/s00382-024-07365-1, 2024.

Payri, C. E., Allain, V., Aucan, J., David, C., David, V., Dutheil, C., Loubersac, L., Menkes, C., Pelletier, B., Pestana, G., Samadi, S., and Sheppard, C.: New Caledonia, in: World Seas: An Environmental Evaluation, edited by: Sheppard, C., Academic Press, 593–618, https://doi.org/10.1016/B978-0-08-100853-9.00035-X, 2019.

Pesin, E., Blaize, S., Lacoste, D., and Argent, M.: Atlas climatique de la Nouvelle-Calédonie, 1995.

Pinazo, C., Bujan, S., Douillet, P., Fichez, R., Grenz, C., and Maurin, A.: Impact of wind and freshwater inputs on phytoplankton biomass in the coral reef lagoon of New Caledonia during the summer cyclonic period: a coupled threedimensional biogeochemical modeling approach, Coral Reefs, 23, 281–296, https://doi.org/10.1007/s00338-004-0378-x, 2004.

Raimbault, P., Lantoine, F., and Neveux, J.: Dosage rapide de la chlorophylle a et des phéopigments a par fluorimétrie après extraction au méthanol. Comparaison avec la méthode classique d'extraction à l'acétone, Océanis : Série de documents océanographiques, 30 (2), 189–205, 2004.

Reid, E. C., DeCarlo, T. M., Cohen, A. L., Wong, G. T. F., Lentz, S. J., Safaie, A., Hall, A., and Davis, K. A.: Internal waves influence the thermal and nutrient environment on a shallow coral reef, Limnology and Oceanography, 64, 1949–1965, https://doi.org/10.1002/lno.11162, 2019.

Roach, C. J., Phillips, H. E., Bindoff, N. L., and Rintoul, S. R.: Detecting and Characterizing Ekman Currents in the Southern Ocean, Journal of Physical Oceanography, 45, 1205–1223, https://doi.org/10.1175/JPO-D-14-0115.1, 2015.

Rodier, M. and Le Borgne, R.: Population dynamics and environmental conditions affecting Trichodesmium spp. (filamentous cyanobacteria) blooms in the south–west lagoon of New Caledonia, Journal of Experimental Marine Biology and Ecology, 358, 20–32, https://doi.org/10.1016/j.jembe.2008.01.016, 2008.

Rodier, M., Pagano, M., Lhomond, L., Péricaud, J.-B., Guilloux, L., Devenon, J.-L., and Chevalier, C.: Effects of physical forcing on short-term plankton dynamics in a narrow coral reef lagoon (Ouano, New Caledonia): a two-week high-frequency study, J Plankton Res, 46, 202–218, https://doi.org/10.1093/plankt/fbae004, 2024.

Rodier, M., Dupouy, C., Domergue, S., Gerard, P., Delepierre, A., Desnues, A., Eldin, G., Fiat, S., and Menkes, C.: MOISE station (Mouillage LagOnaire Instrumenté Suivi BiogéochimiquE): Monthly monitoring of physical and biogeochemical parameters of the waters of the southwest lagoon (New Caledonia), SEANOE, https://doi.org/10.17882/98821, 2026.

Rougerie, F.: Le lagon sud-ouest de Nouvelle-Calédonie: spécificité hydrologique, dynamique et productivité, Editions de l'ORSTOM, Paris, 1986.

Saulia, E., Benavides, M., Henke, B., Turk-Kubo, K., Cooperguard, H., Grosso, O., Desnues, A., Rodier, M., Dupouy, C., Riemann, L., and Bonnet, S.: Seasonal Shifts in Diazotrophs Players: Patterns Observed Over a Two-Year Time Series in the New Caledonian Lagoon (Western Tropical South Pacific Ocean), Front. Mar. Sci., 7, https://doi.org/10.3389/fmars.2020.581755, 2020.

Six, C., Meyneng, M., Ratin, M., Gourvil, P., Siano, R., and Lemonnier, H.: Unravelling the molecular diversity of marine cyanobacterial communities in the lagoon of Nouméa (New Caledonia): impact of a cyclonic event, ISME Commun, 6, ycag032, https://doi.org/10.1093/ismeco/ycag032, 2026.

Specq, D., Bellon, G., Peltier, A., Lefèvre, J., and Menkes, C.: Influence of Subseasonal Variability on the Diurnal Cycle of Precipitation on a Mountainous Island: The Case of New Caledonia, Monthly Weather Review, 148, 333–351, https://doi.org/10.1175/MWR-D-19-0177.1, 2020.

Terry, J. P. and Wotling, G.: Rain-shadow hydrology: Influences on river flows and flood magnitudes across the central massif divide of La Grande Terre Island, New Caledonia, Journal of Hydrology, 404, 77–86, https://doi.org/10.1016/j.jhydrol.2011.04.022, 2011.

Toribio, M. R.-H., Menéndez, A. G., Toribio, S. R.-H., and García, I. Á.: A Novel Approach to Speed Up Hampel Filter for Outlier Detection, Sensors, 25, https://doi.org/10.3390/s25113319, 2025.

Torréton, J.-P., Rochelle-Newall, E., Pringault, O., Jacquet, S., Faure, V., and Briand, E.: Variability of primary and bacterial production in a coral reef lagoon (New Caledonia), Marine Pollution Bulletin, 61, 335–348, https://doi.org/10.1016/j.marpolbul.2010.06.019, 2010.

U.S. Integrated Ocean Observing System: Manual for Real-Time Quality Control of In-Situ Current Observations, U.S. Department of Commerce, National Oceanic and Atmospheric Administration, National Ocean Service, Integrated Ocean Observing System, Silver Spring, MD, https://doi.org/10.25923/sqe9-e310, 2019.

Vincent, E. M., Lengaigne, M., Menkes, C. E., Jourdain, N. C., Marchesiello, P., and Madec, G.: Interannual variability of the South Pacific Convergence Zone and implications for tropical cyclone genesis, Clim Dyn, 36, 1881–1896, https://doi.org/10.1007/s00382-009-0716-3, 2011.

Vincent, E. M., Lengaigne, M., Madec, G., Vialard, J., Samson, G., Jourdain, N. C., Menkes, C. E., and Jullien, S.: Processes setting the characteristics of sea surface cooling induced by tropical cyclones, Journal of Geophysical Research: Oceans, 117, https://doi.org/10.1029/2011JC007396, 2012.

Wang, B., Sun, W., Jin, C., Luo, X., Yang, Y.-M., Li, T., Xiang, B., McPhaden, M. J., Cane, M. A., Jin, F., Liu, F., and Liu, J.: Understanding the recent increase in multiyear La Niñas, Nat. Clim. Chang., 13, 1075–1081, https://doi.org/10.1038/s41558-023-01801-6, 2023.

Wilkinson, M. D., Dumontier, M., Aalbersberg, Ij. J., Appleton, G., Axton, M., Baak, A., Blomberg, N., Boiten, J.-W., da Silva Santos, L. B., Bourne, P. E., Bouwman, J., Brookes, A. J., Clark, T., Crosas, M., Dillo, I., Dumon, O., Edmunds, S., Evelo, C. T., Finkers, R., Gonzalez-Beltran, A., Gray, A. J. G., Groth, P., Goble, C., Grethe, J. S., Heringa, J., ’t Hoen, P. A. C., Hooft, R., Kuhn, T., Kok, R., Kok, J., Lusher, S. J., Martone, M. E., Mons, A., Packer, A. L., Persson, B., Rocca-Serra, P., Roos, M., van Schaik, R., Sansone, S.-A., Schultes, E., Sengstag, T., Slater, T., Strawn, G., Swertz, M. A., Thompson, M., van der Lei, J., van Mulligen, E., Velterop, J., Waagmeester, A., Wittenburg, P., Wolstencroft, K., Zhao, J., and Mons, B.: The FAIR Guiding Principles for scientific data management and stewardship, Sci Data, 3, 160018, https://doi.org/10.1038/sdata.2016.18, 2016.

Wong, A., Keeley, R., and Carval, T.: Argo Quality Control Manual for CTD and Trajectory Data, https://doi.org/10.13155/33951, 2025.

Wunsch, C. and Stammer, D.: Atmospheric loading and the oceanic “inverted barometer” effect, Reviews of Geophysics, 35, 79–107, https://doi.org/10.1029/96RG03037, 1997.

Wyatt, A. S. J., Leichter, J. J., Toth, L. T., Miyajima, T., Aronson, R. B., and Nagata, T.: Heat accumulation on coral reefs mitigated by internal waves, Nat. Geosci., 13, 28–34, https://doi.org/10.1038/s41561-019-0486-4, 2020.